Sensors & Diagnostics

CRITICAL REVIEW

View Article Online
View Journal | View Issue

Cite this: *Sens. Diagn.*, 2024, **3**, 893

Advances in electrochemical sensors for real-time glucose monitoring

Md. Harun-Or-Rashid, †[a] Most. Nazmin Aktar, †[a] Veronica Preda [b] and Noushin Nasiri *[cd]

Received 18th March 2024,
Accepted 1st May 2024

DOI: 10.1039/d4sd00086b

rsc.li/sensors

Technological advancements are revolutionizing diabetic care worldwide, particularly in the realm of glucose monitoring. Traditionally invasive and cumbersome, glucose monitoring is shifting towards less invasive methods, enhancing patient quality of life and reducing risks associated with hypo- and hyperglycemia. Wearable biosensors, focusing on sweat and interstitial fluid, offer novel avenues for early disease detection and personalized point-of-care testing. This review paper provides a comprehensive overview of recent strides in wearable sweat sensors, including historical perspectives, electrochemical sensing mechanisms, material advancements, and the role of nanomaterials in enhancing sensor performance. By examining the evolution of glucose monitoring devices and highlighting commercially available devices, the review underscores the wide-ranging utility of electrochemical sensors in glucose monitoring. Enzymatic and non-enzymatic sensing mechanisms, potentiometric, amperometric/voltammetric sensors, ion-selective electrodes, and biosensors are discussed in detail, alongside various materials employed to optimize sensor performance. The burgeoning interest in nanomaterial-enabled sensor platforms signifies a promising future for sweat-based glucose monitoring, with potential implications for personalized healthcare and disease management.

[a] *Department of Applied Chemistry, Graduate School of Engineering, University of Hyogo, 2167 Shosha, Himeji 671-2280, Hyogo, Japan*
[b] *Department of Endocrinology, Faculty of Health and Human Sciences Macquarie University, Sydney 2109, Australia*
[c] *NanoTech Laboratory, School of Engineering, Faculty of Science and Engineering, Macquarie University, Sydney 2109, Australia. E-mail: noushin.nasiri@mq.edu.au*
[d] *Smart Green Cities Research Centre, Macquarie University, Sydney 2109, Australia*
† Co-first author.

Introduction

Technological advances are revolutionizing diabetic care across the globe.[1] In diabetic patients, regular glucose monitoring is needed to optimize control and reduce glycaemic variability.[2] This has been in the past very invasive, cumbersome and blood based. Such testing by less invasive means has the ability to reduce the risks of hypo and

Md. Harun-Or-Rashid

Md. Harun-Or-Rashid received his B.Sc. and M.Sc. degrees in Pharmacy in 2018 and 2020, respectively, from Daffodil International University, Dhaka, Bangladesh. From 2019 to 2022, he was a training executive at a pharmaceutical company in Bangladesh. Later, wanting to further his academic pursuits he joined the Department of Chemistry at the University of Hyogo, Graduate School of Engineering in Hyogo, Japan, as a research student having received the prestigious Japanese Government MEXT scholarship, working in the area of polymer synthesis.

Most. Nazmin Aktar

Most. Nazmin Aktar obtained her B.Sc. in 2020 and subsequently her Masters (M.Sc.) from Daffodil International University, Dhaka in 2022. In 2023, she furthered her academic pursuites at the Department of Applied Chemistry, University of Hyogo, Graduate School of Engineering in Hyogo, Japan, in the role of a research assistant. Her research interests focus on polymer synthesis and the modification of Resovist using poly(2-methacryloyloxyethyl phosphorylcholine) (PMPC) polymer.

hyperglycaemia, and improve patient quality of life for a wide range of patient populations.[3] Wearable biosensors, with a focus on sweat and interstitial fluid (ISF) as abundant sources of biochemical markers,[4,5] offer pioneering avenues for management as well as early disease detection and personalized point-of-care testing (POCT).[6–10] These sensors afford real-time physiological data acquisition through noninvasive means, enabling continuous monitoring round the clock.[11] For instance, the accurate surveillance of hypoglycemia or hyperglycemia *via* sweat is essential for diabetic patients, as fluctuations in blood glucose levels pose significant health risks.[12]

Diabetes is a leading cause of chronic disease, with 530 million people globally (1 in 10 adults) affected.[13] It is characterized by erratic blood glucose levels and ranks among the foremost causes of global mortality. Due to the associated burden of disease, access to care and painful finger-prick testing there can be non-compliance with monitoring. In the short term there are the physiological complications of hypoglycaemia or hyperglycaemia (DKA or HONK) and longer term the risk of severe complications such as cardiovascular disease, renal impairment, vision impairment, and neuropathies. Glycaemic variability has been shown to be associated with greater microvascular disease. Therapeutic options focus on titrating medications to achieve greater time in range (TIR).[14]

Type 1 diabetic (T1D) patients have autoimmune destruction of their pancreatic beta-cells, reliant on insulin and are routinely advised to monitor their blood sugar levels daily and administer insulin subcutaneously *via* syringe, prefilled pens or insulin pump devices.[15] Type II diabetic (T2D) patients are typically insulin resistant requiring a number of medications orally and or injected (including insulin in some patients) to control their blood glucose levels.[16] The World Health Organization (WHO) has also updated the diabetes classification to reflect the presence of many other forms of diabetes including hybrid forms of diabetes, specifically LADA ('type 1.5 diabetes') which has features of both T1D and T2D.[17] Excess insulin or other glucose lowering therapy over titration can precipitate perilous hypoglycemic episodes, potentially culminating in coma or fatality. Presently, interstitial monofilament sensors serve as the primary means of glucose monitoring, albeit with inherent limitations including invasiveness, finite lifespan, high costs, compatibility issues, signal lag, and dermal reactions.

The integration of nanotechnology has become crucial in enhancing sensitivity on detector surfaces for biomarker detection. This advancement has resulted in a significant increase in the lower limit of detection by a thousand-fold, offering novel opportunities to enhance selectivity while reducing power consumption. Early research in non-invasive diabetes diagnostics has illustrated the feasibility of this approach through breath analysis. Utilizing straightforward solid-state devices composed of distinct nanomaterial compositions, it is now possible to detect acetone, the primary breath marker for diabetes, in human breath at extremely low concentrations, reaching down to a few particles per billion.[18–20] Furthermore, through nanostructuring and functionalization of electrochemical micro-electrodes integrated into flexible polymer substrates, real-time measurement of glucose and other vital biomarkers directly from human tears, saliva and sweat has become achievable.[21–23] Technological innovations in electrochemical sweat sensors offer promising solutions to circumvent these constraints by enabling multiplexed sensing for concurrent detection of diverse analytes, employing iontophoresis for sweat induction, and integrating microfluidic systems for precise measurements.[24,25] Moreover, self-powered wearable

Veronica Preda

Associate Professor Preda is Head of MQ Health Endocrinology and Clinical Lead of MD Research at Macquarie University Sydney Australia. She has over 160 publications and presentations including 4 book chapters across a breadth of medical research over the last 20 years. She completed a Fellowship at the Oxford Centre for Diabetes, Metabolism and Endocrinology in the UK where she worked on the genetic basis of central nervous system tumours. She has a Masters of Public Health from the University of New South Wales and is actively involved in medical student through to post graduate teaching, PhD supervision, Physician specialist training and collaborates in multiple international clinical trials.

Noushin Nasiri

Associate Professor Noushin Nasiri is the head of NanoTech Laboratory and the deputy director of Smart Green Cities Research Centre at Macquarie University. Her research team is focused on design and fabrication of nanostructured materials, functionalised coatings, miniaturized sensing technologies and wearable devices for health, energy and environmental applications. She is the recipient of 2023 NSW Cancer Institute Fellowship, 2022 L'Oréal-UNESCO For Women in Science Fellowship, 2021 Royal Society of New South Wales Warren Prize and 2019 NSW Young Tall Poppy Science Award.

sensors, leveraging energy harvesting and storage mechanisms, ensure sustainable and autonomous operation, generating extensive time-series data that underpin personalized and intelligent healthcare *via* big-data analytics.[26,27]

Electrochemical sensors represent pivotal components in noninvasive sweat glucose monitoring devices, functioning on the principles of electrochemistry to detect and quantify specific chemical compounds. These sensors typically comprise a working electrode, a reference electrode, and an electrolyte (Fig. 1a and b), where the working electrode (WE) facilitates the electrochemical reaction with the target analyte, while the reference electrode (RE) maintains a stable potential for accurate measurements.[22] The electrolyte facilitates ion flow between electrodes, and the sensing mechanism involves redox reactions wherein the target analyte undergoes oxidation or reduction at the working electrode. Potentiometric sensors (Fig. 1a) measure the potential difference between working and reference electrodes,[28] providing quantitative insights into analyte concentrations,[29] while amperometric sensors (Fig. 1b) gauge the current generated during electrochemical reactions, offering an alternative approach for quantification.[24,30] Ion-selective electrochemical sensors are a sub-class of potentiometric sensors that operate based on specific ion-membrane interactions, selectively responding to desired ions for concentration quantification.[31] Enzyme-based electrochemical sensors (Fig. 1c) amalgamate enzyme specificity with electrochemical transduction principles to detect and quantify specific analytes, with enzyme selection crucially dictating sensor specificity.[32] Non-enzyme-based electrochemical sensors (Fig. 1d) utilize alternative transduction principles, such as direct oxidation–reduction reactions or nanomaterial-based mechanisms, to detect and quantify analytes without relying on enzyme specificity.[33,34] It should be noted that the reaction pathway depicted in Fig. 1d represents a simplified model designed to illustrate a general non-enzyme-based electron transfer mechanism. Consequently, it may not fully capture the complexity inherent in all such reactions.[35]

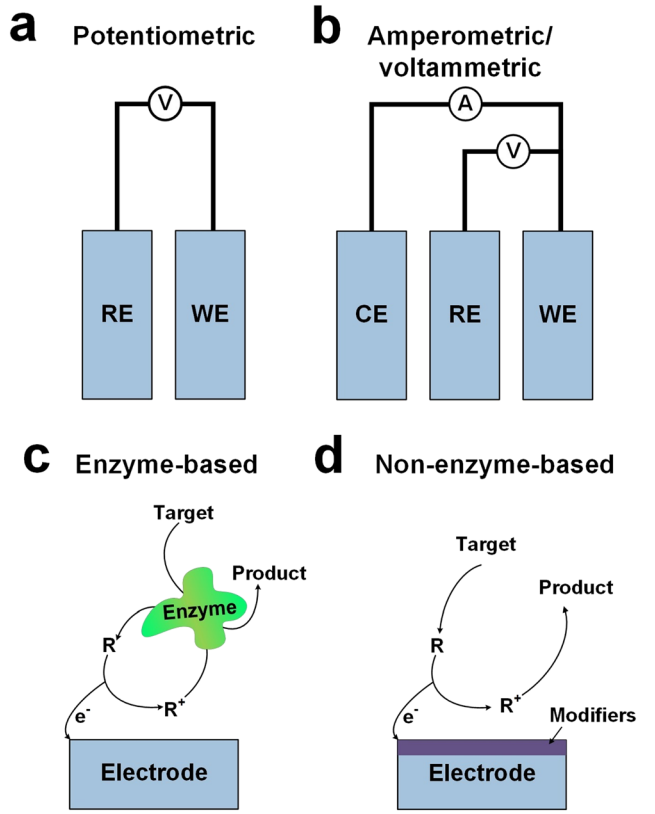

Fig. 1 Schematic diagram of a) potentiometric, b) amperometric/voltammetric, c) enzyme-based and d) non-enzyme-based electrochemical sensors (note: the pathway for non-enzyme-based sensors illustrated here represents a generalized mechanism, and specific reactions may involve direct electron transfer from the target to the electrode or through different intermediaries).

This review aims to comprehensively overview of recent strides in wearable sweat sensors, encompassing historical perspectives, electrochemical sensing mechanisms, and material advancements. We summarize the evolution of glucose monitoring devices from inception to contemporary developments, alongside deliberating on the United States Food and Drug Administration (FDA)-approved commercially available glucose sensing devices. Subsequently, our review expands on the wide-ranging utility of electrochemical sensors in glucose monitoring devices, elaborating on both enzymatic and non-enzymatic sensing mechanisms, potentiometric and amperometric sensors, ion-selective electrodes, and biosensors. Finally, we highlight various materials employed in electrochemical sensors to facilitate sensing processes and optimize sensor performance.

Historical background of wearable glucose biosensors

Wearable biosensors have catalyzed advancements across diverse domains by enabling continuous, real-time monitoring of physiological parameters through non-invasive assessment of biochemical markers in biofluids such as sweat, tears, saliva, and interstitial fluid.[21–23] These biosensors typically comprise a biological recognition layer interfacing with target molecules and a transducer effecting the conversion of molecular interactions into quantifiable signals. Sweat-based sensors, in particular, offer unparalleled convenience owing to the facile accessibility and collection protocols associated with sweat.[25] Employing components such as receptors, nucleic acids, cells, and enzymes, these sensors leverage optical, colorimetric, or acoustic sensing modalities.[24,25] Mechanistically, these sensors facilitate analyte collection *via* microfluidic mechanisms, followed by detection through a bio-recognition layer, signal transduction, and subsequent wireless or local output presentation.[36,37]

Fig. 2 outlines the evolution of biosensors for wearable applications, from their beginnings to very recent years.[38] Initially focused on monitoring blood glucose levels using

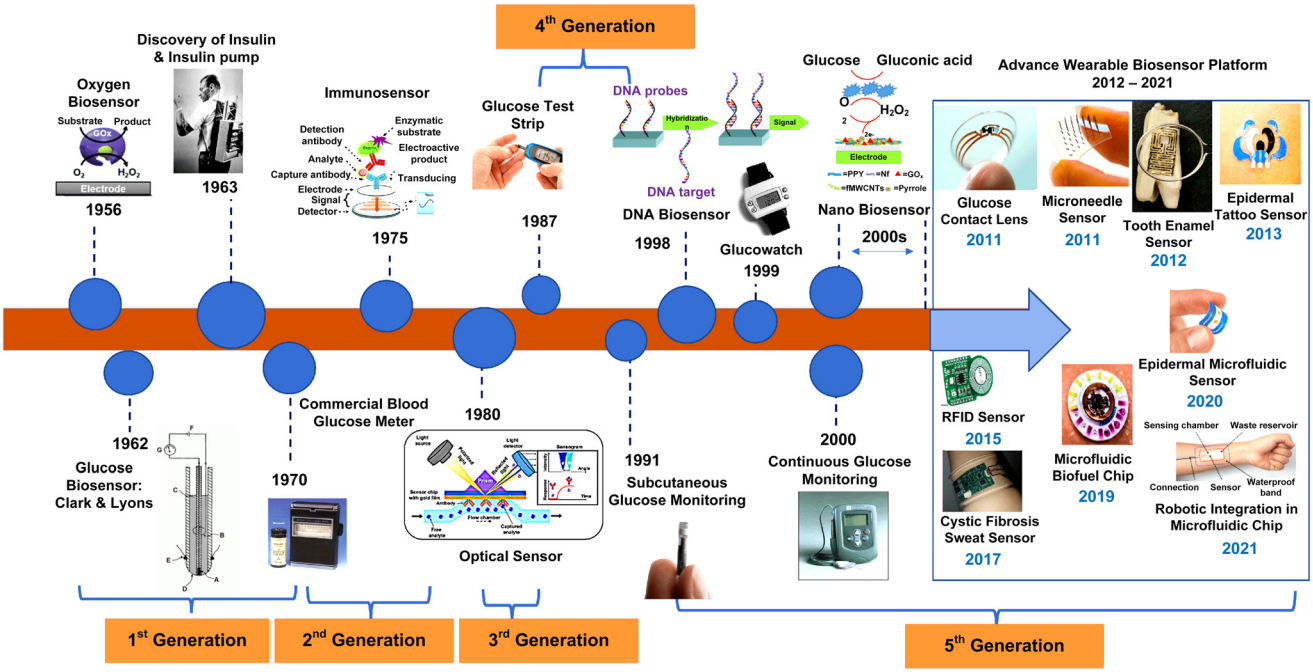

Fig. 2 Evolution of biosensors for wearable applications from beginnings to the present day (adapted with permission from ref. 38, copyright 2022, MDPI).

enzyme-based electrodes, the field saw a significant breakthrough in the 1962 with the introduction of glucose-oxidase-enzyme-based biosensors by Clark and Lyons.[39] These biosensors facilitated the monitoring of glucose levels through enzymatic reactions, leading to the development of the first-generation glucose sensor. Over time, improvements such as immobilization of enzymes and the introduction of insulin pumps by Kadish[40] in 1963 enhanced blood glucose management, despite some logistical challenges. The expression of glucose oxidase has notably advanced the development of electrochemical sensors for glucose monitoring, as evidenced by the myriad of designs and implementations that followed. The original glucose oxidase enzyme electrode by Updike and Hicks,[41] intended for continuous blood glucose monitoring, marked a significant milestone. This enzyme electrode employed amperometric methods to measure oxygen depletion in an immobilized glucose oxidase gel, demonstrating an innovative approach to glucose sensing. Throughout the mid-20th century, pioneers like Leland C. Clark and Arnold Kadish made significant contributions to biosensor technology, culminating in the development of the first glucose meter, Dextrostix, in the 1970s.[42] These innovations laid the groundwork for home blood glucose monitoring, transforming diabetes management.

In the 1990s, George S. Wilson's needle-type glucose sensors revolutionized glucose sensing technology,[43] improving precision, selectivity, and patient comfort. Concurrently, advancements in DNA sensor technology[44] and nanotechnology further expanded biosensing capabilities, leading to the development of continuous glucose monitoring (CGM) devices and nanomaterial-based biosensors. The COVID-19 pandemic since March 2020 has accelerated the adoption of telehealth and virtual diabetes care, with continuous glucose monitors (CGM) and insulin pumps playing a central role in remote data accessibility.[45,46] The FDA has been instrumental in authorizing the use of emerging technologies for patient and healthcare provider access. See Table 1 and Fig. 3 for an overview of FDA-approved glucose monitoring devices.

In recent years, there has been a burgeoning interest in leveraging nanomaterials to pioneer the development of cutting-edge electrochemical sensors for glucose monitoring in sweat.[24,32,47–49] This surge in research activity has resulted in the exploration of a diverse array of nanomaterials, ranging from carbon-based materials[50] such as graphene[51,52] and carbon nanotubes[53,54] to metal-based nanoparticles like gold[47,55] and silver.[56,57] These nanomaterials possess unique properties such as high surface area, exceptional conductivity, and catalytic activity, rendering them highly suitable for enhancing the performance of glucose sensors.[23,58] Through a detailed exploration of these nanomaterial-enabled sensor platforms, this review aims to provide valuable insights into the burgeoning field of sweat-based glucose monitoring and its potential implications for personalized healthcare and disease management.

Carbon-based electrochemical sensors

Carbon-based electrochemical sensors exploit the distinctive electrochemical characteristics of carbon-based materials,[59] including carbon nanotubes (CNTs),[60–62] graphene,[63,64] and

Table 1 FDA approved glucose monitoring devices

Device name	Type	Description	Year of approval
Dexcom G6 (Fig. 3a)	CGM	Provides real-time glucose readings every 5 minutes; worn as a sensor on the body with a transmitter that sends data to a receiver or smartphone app	2019
Accu-Chek Guide (Fig. 3b)	Blood glucose meter	Provides easy-to-use features like spill-resistant vial, large test strip dosing area, and connectivity options	2016
OneTouch Verio Flex (Fig. 3c)	Blood glucose meter	Offers accurate blood glucose readings; may include features like wireless data syncing with compatible apps	2016
Abbott FreeStyle Libre (Fig. 3d)	Flash GM	Measures interstitial fluid glucose levels; users scan the sensor with a reader or smartphone to obtain glucose readings; does not require routine fingerstick calibrations	2022
Medtronic MiniMed 670G (Fig. 3e)	Hybrid closed-loop	Insulin pump system that automatically adjusts basal insulin delivery based on CGM readings to maintain glucose levels within a target range	2017
Medtronic Guardian Sensor 3 (Fig. 3f)	CGM	Provides real-time glucose data; integrated with Medtronic insulin pumps to aid in diabetes management	2018

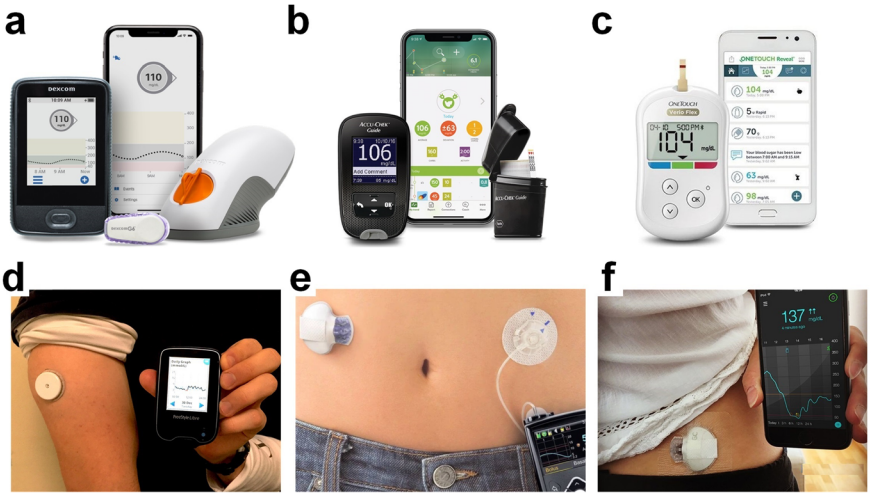

Fig. 3 The glucose monitoring devices approved by the US-FDA for patient and healthcare provider access: a) Dexcom G6, b) Accu-Chek Guide, c) OneTouch Verio Flex, d) Abbott FreeStyle Libre, e) Medtronic MiniMed 670G, and f) Medtronic Guardian Sensor 3.

carbon quantum dots[65,66] to enable efficient analyte detection. CNTs, exemplifying sp^2 carbon structures composed of graphene sheets arranged as molecular cylinders, exist predominantly in three forms: single-walled carbon nanotubes (SWCNT), double-walled carbon nanotubes (DWCNT), and multi-walled carbon nanotubes (MWCNTs).[67] These nanostructures exhibit notable attributes such as high chemical and thermal stability, low capacitance, enhanced peak currents, and reduced overpotentials, all of which enhance sensor sensitivity.[68,69] Yun Oh *et al.*[70] developed a skin-attachable, stretchable electrochemical sensor employing CNTs for the detection of glucose and pH in sweat using a simple, cost-effective layer-by-layer (LbL) method.[71] The sensor's assembly comprised three sequential steps: first, employing gold nanostructures (AuNS) to create an intrinsically stretchable sensor platform devoid of serpentine or island-bridge structures; second, depositing CNTs onto the AuNS substrate *via* LbL method (Fig. 4a); and finally, fabricating a glucose-detecting WE by depositing a $CoWO_4$/CNT nanocomposite onto the LbL-CNT/AuNS platform through LbL deposition, eliminating the need for enzyme utilization. $CoWO_4$ nanoparticles were hydrothermally synthesized on the CNT surface (Fig. 4a), offering high conductivity and a substantial surface area. A pH-sensitive electrode based on polyaniline (PANI), was fabricated *via* electropolymerization on the LbL-CNT film, leveraging PANI's pH-sensitive properties resulting from surface deprotonation enabling hydrogen ion detection.[70] The integration of adhesive materials like silbione facilitated the development of a skin-attachable sweat sensor (Fig. 4b). The sensor exhibited commendable performance metrics, with sensitivities of 10.89 μA mM^{-1} cm^{-2} and 71.44 mV per pH for glucose and pH, respectively (Fig. 4c and d), coupled with mechanical stability up to 30% stretching (Fig. 4b, inset) and air stability for 10 days. The sensor demonstrated strong adhesion even in wet skin conditions, enabling the detection of glucose and pH levels in sweat during physical activities such as running while adhered to the skin.

Garland *et al.*[72] fabricated wearable flexible perspiration biosensors using laser-induced graphene (LIG)[73,74] in

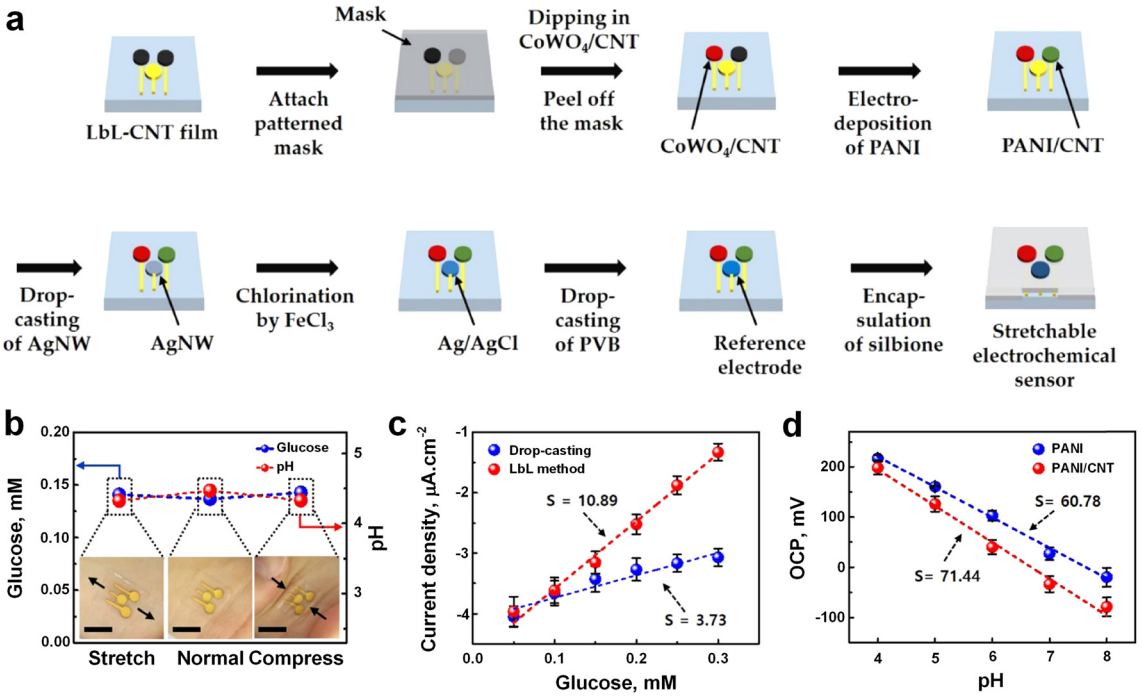

Fig. 4 a) Schematic of the fabrication processes using LBL deposition to prepare a skin-attachable, stretchable electrochemical sweat sensor. b) Assessment of the effectiveness of the skin-attached sensor in human sweat during mechanical deformation to determine glucose and pH levels. c) Sensing performance of the sensor fabricated by drop-casting (blue), and LBL (red) techniques toward glucose. d) Sensing performance of pH senor PANI (blue), and PANI/CNT (red) fabricated pH sensor (adapted with permission from ref. 70 copyright 2018, American Chemical Society).

combination with polymeric tape microfluidics for continuous monitoring of glucose in medical diagnostics and athletic performance assessment. The working, reference, and counter electrodes were customized in shape and dimensions to suit the dimensions of microfluidic patches (Fig. 5a and b). Initially, the sensors underwent *ex vivo* testing using a microfluidic setup that delivered artificial perspiration containing target biomarkers to the sensors *via* laser-drilled holes, emulating the size and distribution of human skin pores. Subsequent on-body evaluation was conducted during cycling exercises in a multi-subject trial involving 15 participants with varying demographics. *In vitro* assessments revealed a glucose sensitivity of 26.2 μA mM^{-1} cm^{-2} and a detection limit of 8 μM in phosphate-buffered saline (PBS) (Fig. 5c, red line). Sensitivity was slightly lower in artificial sweat (Fig. 5c, blue line) due to variations in pH and ionic strength, resulting in a sensitivity of 12.6 μA mM^{-1} cm^{-2} and a detection limit of 47.7 μM. Individual sensor repeatability was also excellent with R^2 = 0.99 and low error bars (sd. $<1.0 \times 10^{-7}$) at all concentrations (Fig. 5d). Comparative analysis with existing wearable glucose sensors showcased superior performance, coupled with reduced costs and complexity, underscoring the potential of LIG-based glucose biosensors for wearable applications.

MOF-based electrochemical sensors

MOFs have emerged as highly promising materials across various applications owing to their exceptional properties.[75,76] One such application is in the realm of wearable glucose sensors,[77] which hold significant potential for continuous glucose level monitoring in individuals afflicted with diabetes, offering real-time data acquisition without the necessity for frequent blood sampling.[49,56] Shu *et al.*[56] have developed a highly stretchable wearable electrochemical sensor employing Ni–Co metal–organic framework/Ag/reduced graphene oxide/polyurethane (Ni–Co MOF/Ag/rGO/PU) (NCGP) to continuously and accurately measure glucose levels in sweat. The fabrication process involved an enhanced wet spinning technique to produce reduced graphene oxide/polyurethane (rGO/PU) fibers using a capillary template. These fibers (rGO/PU) were subsequently coated with conductive Ag glue and Ni–Co MOF nanosheets, resulting in a stretchable fiber WE (Fig. 6a). Comparative electrochemical analysis revealed that the NCGP fiber electrode exhibited superior performance for glucose detection compared to conventional rGO/PU and Ag/rGO/PU fiber electrodes due to its enhanced electrocatalytic activity. The NCGP fiber electrode demonstrated sustained electrochemical performance even under mechanical deformation, underscoring its exceptional stretchability and durability. The integration of the NCGP fiber electrode, Ag/AgCl fiber reference electrode, and Pt wire CE onto absorbent fabric, fixed onto stretchable PDMS substrate, facilitated the creation of a wearable nonenzymatic sweat glucose sensor (Fig. 6b), which was subsequently deployed on a volunteer's arm for glucose level monitoring (Fig. 6c). Electrocatalytic activity analysis on the flexible NCGP fiber electrode elucidated its

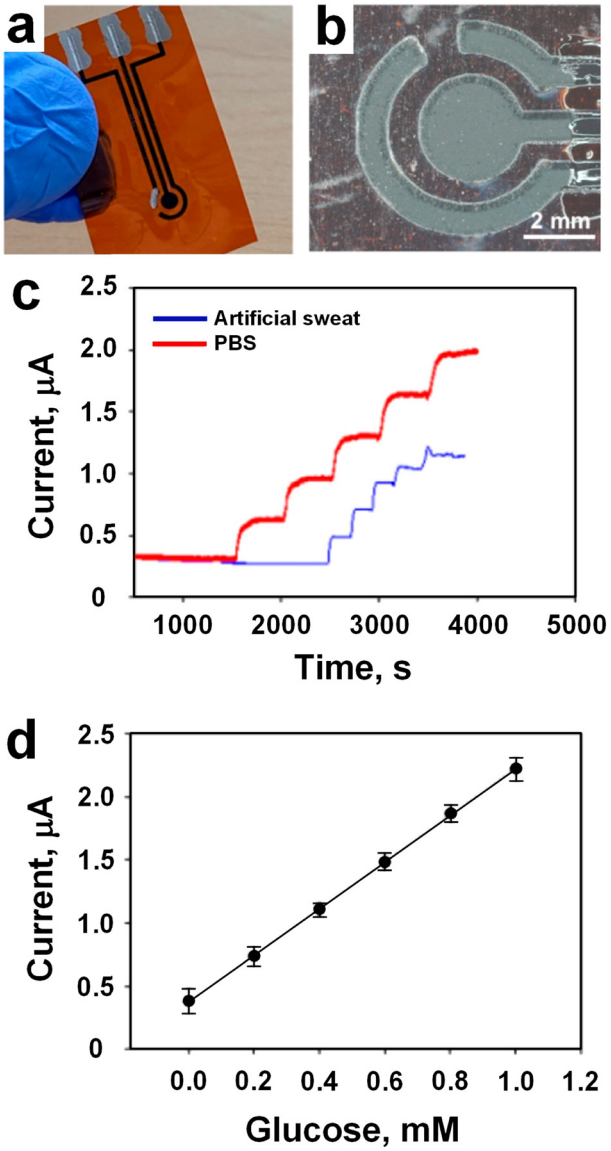

Fig. 5 a) Image of an amperometric LIG sensor with three electrodes. b) Microscopic image showing working, reference, and counter electrodes protecting the LIG electrical leads. c) LIG glucose biosensor tests in artificial sweat, and PBS. d) Individual glucose sensor dynamic range and repeatability for n = 3 (values presented as average ± standard deviation) (adapted with permission from ref. 72, copyright 2023, American Chemical Society).

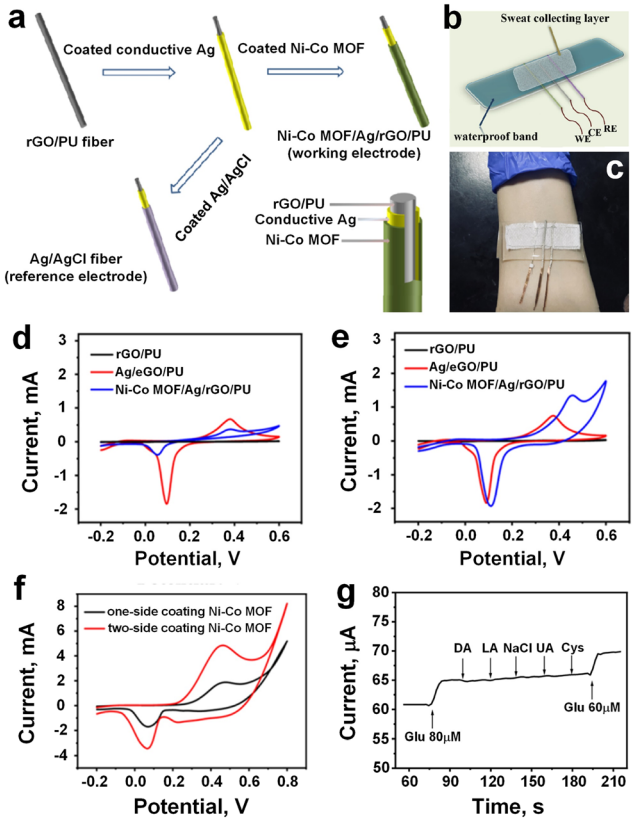

Fig. 6 a) Schematic presentation of the manufacturing process to WE (NCGP), and RE (Ag/AgCl Fiber). b) Schematic diagram of NCGP glucose sensor integrated into the stretchable PDMS substrate. c) Sensing device attached to the volunteer's arm. d) CV curves of different fiber electrodes in 0.1 M NaOH without glucose. e) CV curves of different fiber electrodes in 0.1 M NaOH with 0.1 mM glucose. f) Comparison of the one-side coated Ni–Co MOF, and two-side coated Ni–Co MOF electrode against redox peak current. g) Glucose sensitivity after addition various interference substances (adapted with permission from ref. 56 copyright 2021, American Chemical Society).

superior performance in glucose oxidation compared to other electrodes, as evidenced by cyclic voltammetry (CV) responses (Fig. 6d and e). Furthermore, an investigation into the impact of Ni–Co MOF coating configuration revealed that double-sided coating led to a twofold increase in redox peak current due to the higher electroactive surface area (Fig. 6f). Additionally, varying concentrations of glucose resulted in corresponding changes in oxidation current, indicating the efficacy of Ni–Co MOF in facilitating glucose oxidation over a wide concentration range.

Amperometric analysis demonstrated the excellent glucose detection performance of the NCGP fiber electrode, exhibiting a linear range of 10 μM to 0.66 mM, high correlation coefficient (R^2 = 0.9873), and sensitivity of 425.9 μA mM^{-1} cm^{-2}. Moreover, the sensor displayed good selectivity for glucose detection amidst various interfering substances like DA, LA, NaCl, UA, and Cys (Fig. 6g), and exhibited minimal sensitivity to temperature changes during glucose detection. Comparative analysis against other flexible electrochemical glucose sensors revealed the superior sensing performance of the NCGP-based sensor, which maintained consistent sensitivity even under mechanical deformation, along with long-term stability and minimal sensitivity to temperature fluctuations. Validation against commercial glucose meters confirmed the accuracy of the NCGP fiber-based wearable sensor in detecting glucose levels in sweat, thus highlighting its efficacy for real-world application.

Very recently, Xia *et al.*[49] engineered a wearable electrochemical sensor utilizing a bimetallic (Ni–Co) MOF-coated CNT/PDMS film electrode employing a dual-stamping method for real-time analysis of sweat glucose levels. They presented a facile approach, termed stamping-vacuum

filtration dry transfer (SVFDT) method, for the fabrication of a wearable sweat glucose sensor incorporating CNTs/MWCNTs/PDMS (CMP). A WE, made of Ni–Co MOF/CNTs/MWCNTs/PDMS (NCMP), was prepared by selectively modifying the enzyme-like Ni–Co MOF material onto the active region of the electrode, and NCMP has three electrodes such as RE, CE, and WE (Fig. 7a). The sensor patch was fixed above the volunteers' arm to absorb sweat for detection (Fig. 7b) while indoor exercise was performed for 20 min before the test to collect sweat. Comparative CV analysis of CMP and NCMP film electrodes before glucose introduction revealed a significant increase in oxidation current specifically for the NCMP film electrode upon the addition of glucose, suggesting the superior catalytic activity of Ni–Co MOF nanomaterials towards glucose oxidation and its accurate detection. The gradual addition of glucose (from 20 μM to 1100 μM) resulted in a proportional increase in oxidation peak current for the NCMP film electrode (Fig. 7c), indicating facile glucose oxidation over a wide concentration range. Sensitivity assessment using the amperometry method demonstrated rapid current escalation with rising glucose concentration, showcasing the excellent sensitivity of the flexible NCMP film electrode-based sensor. Calibration curves revealed an outstanding correlation coefficient (R^2 = 0.998) with a linear range spanning from 20 μM to 1.1 mM for the NCMP film electrode (Fig. 7d), accompanied by a remarkable sensitivity of 71.62 μA mM^{-1} cm^{-2} and a low detection limit of 6.78 μM (signal/noise = 3) for glucose detection.

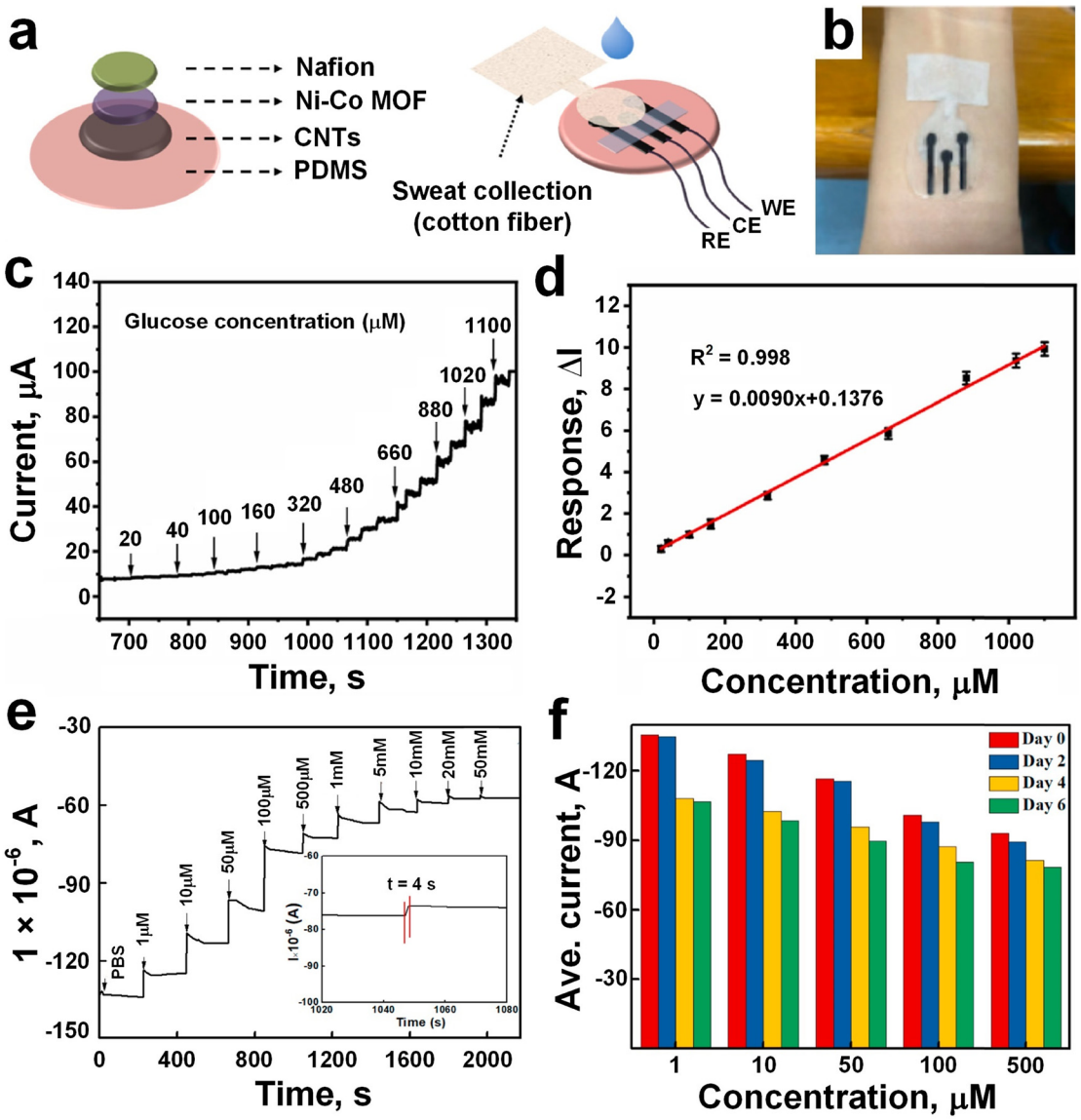

Fig. 7 a) NCMP glucose sensor preparation, and integrated with RE, CE, and WE. b) The sensor was fixed above the volunteers' arms to absorb sweat for detection. c) The oxidation time–current curve against series of glucose concentration (20–1100 μM). d) Calibration curve NCMP current response against different glucose concentration (adapted with permission from ref. 49 copyright 2023, Elsevier). e) Glucose detection test with different concentration range between 1–50 mM. f) The current signals of the GOD–GA–Ni/Cu-MOFs electrode dropped after two, four, and six days, respectively (adapted with permission from ref. 78 copyright 2021, Elsevier).

Furthermore, selectivity evaluation of the NCMP film electrode for glucose detection against various active interfering substances commonly present in sweat (*e.g.*, lactate, uric acid, sodium chloride, ascorbic acid) illustrated that only glucose elicited a significant impact on the current signal, affirming the excellent selectivity of the film electrode.

In a similar approach, Wang *et al.*[78] developed a glucose sensor employing a field-effect transistor (FET) configuration integrated with bimetallic Ni/Cu-MOFs. A one-step hydrothermal method was employed to fabricate a novel glucose biosensor, wherein Ni/Cu-MOFs films were directly grown on FET devices and functionalized with GO_x using glutaraldehyde (GA) as a linker. Various ratios of Ni and Cu ions (ranging from 1 : 7 to 30 : 1) were investigated to discern their influence on the characteristics of the bimetallic MOFs. The biosensor's field-effect performance and glucose detection capabilities were systematically assessed, contrasting with sensors based on monometallic Ni-MOFs. The Ni/Cu-MOFs-based biosensor manifested enhanced electrical conductivity and specific responsiveness to glucose, even amidst the presence of interfering substances (such as sucrose, fructose, uric acid, ascorbic acid, galactose, and lactose), underscoring its significant potential for glucose detection. The gradual increase in glucose concentration, spanning from 1 μM to 50 mM, led to a notable shift in the source-drain current of the GO_x–GA–Ni/Cu-MOFs (7 : 1)-FET (Fig. 7e), with a fast response dynamic of less than 5 seconds (Fig. 7e, inset). The underlying cause was traced back to the enzymatic reaction occurring between glucose and GOD, which resulted in a transient modification of the protonation state within the conductive MOFs. Comparative analysis against other FET-based glucose sensors[79–81] showcased superior sensitivity, broader detection range, and lower detection limit for the GO_x–GA–Ni/Cu-MOFs (7 : 1)-FET (*e.g.*, the sensitivity of 26.05/10.96 μA μM^{-1} cm^{-2}, the detection range of 0.001–20 mM, the detection limit of 0.51 μM). Moreover, the biosensor demonstrated a low standard deviation of 3.32% in glucose detection, indicative of its robust reliability. Despite exhibiting less favorable long-term stability (Fig. 7f), where the sensitivity dropped by 2.12%, 16.72% and then 20.60% by the second, fourth and sixth days of testing, respectively, the GO_x–GA–Ni/Cu-MOFs-FET could be utilized as a disposable and real-time glucose sensor due to its commendable specificity, reproducibility, and rapid response time.

Polymeric-based electrochemical sensors

Polymeric-based electrochemical sensors have garnered significant attention and recognition in recent years due to their versatility, adaptability, and inherent properties (*e.g.* flexibility, biocompatibility, and tunable conductivity) conducive to sensing applications.[82,83] With advances in polymer science and electrochemical techniques, polymeric-based sensors exhibit enhanced sensitivity, selectivity, and stability, making them invaluable tools in fields ranging from biomedical diagnostics[84,85] to environmental monitoring.[86,87] Commonly employed polymers encompass a diverse range of materials tailored to specific sensor requirements: PDMS serves as a flexible substrate,[88–90] polyethylene terephthalate (PET) facilitates textile integration,[90–93] polyimide (PI) imparts thermal stability,[94–96] PU enhances mechanical properties,[97,98] polyvinyl alcohol (PVA) enables hydrogel-based sensing,[99,100] polyacrylamide (PAM) ensures biocompatibility,[101,102] and conductive polymers such as poly(3,4-ethylene dioxythiophene):poly(styrene sulfonate) (PEDOT:PSS), PANI, and polypyrrole (PPy) offer superior electrical conductivity.[103,104] These diverse polymeric materials collectively enable the development of wearable sensors characterized by comfort, conformability, and accuracy in detecting sweat analytes such as glucose, electrolytes, and metabolites. Through strategic selection and integration of these polymers, wearable sweat sensors can achieve optimal performance and versatility, catering to a wide array of biomedical and healthcare applications.

Conductive polymers

Conductive polymers present a versatile framework for the advancement of wearable sweat sensors,[105–107] offering augmented performance metrics including flexibility and biocompatibility, thus rendering them highly promising across a spectrum of applications encompassing healthcare, sports performance monitoring, and personalized wellness management. These sensors typically integrate conductive polymers either as sensing elements or as constituents of the electrode system to discern and quantify diverse analytes within sweat. PANI stands as a pivotal subject of investigation in the realm of conducting polymers[108] and its appeal lies in several inherent advantages, including notable thermal and environmental stability, elevated conductivity, and straightforward and cost-effective synthesis methodologies.[109] Recently, Lim *et al.*[110] developed a wearable sweat biosensor featuring a pliable nanocomposite layer made of nitrogen-doped graphene quantum dots (N-GQDs) onto the PANI for glucose monitoring. The inclusion of N-GQDs facilitated enhanced electron transfer, consequently endowing the N-GQDs/PANI nanocomposite with heightened sensitivity towards H_2O_2 in comparison to pristine PANI. This enhancement culminated in sensitivity values of 68.1 ± 1.11 and 44.06 ± 2.1 μA mM^{-1} cm^{-2} for N-GQDs/PANI and pristine PANI, respectively. Moreover, upon integration of GO_x, the GO_x/N-GQDs/PANI-based biosensor exhibited exemplary performance in glucose detection within artificial sweat. Even when incorporated into a flexible electrode, precise glucose detection was upheld, with the sensitivity of 93.2% without any discernible alterations in the nanocomposite layer's morphology. In contrast, the sensitivity of the GO_x/Pt-based biosensor dwindled to 71.3% for glucose detection post continuous bending tests. Consequently, the N-GQDs/PANI

nanocomposite layer ensured steadfast long-term monitoring with resilient electrodes for non-invasive human sweat glucose monitoring using wearable biosensors. In a similar approach, Chang *et al.*[111] made a novel NGQDs/PANI for a non-invasive wearable self-powered triboelectric sensor (TES) aimed at monitoring glucose levels in human sweat. By introducing electron-rich functional groups such as NGQDs, the surface electronegativity of PANI was modulated (Fig. 8a and b), fostering enhanced charge transfer between PANI and intermediates, and amplifying triboelectric outputs. Fig. 8b showed the schematic illustration for the working principle of zeta potential measurement for thin films by surface potential analyzer. The presence of GO_x in NGQDs/PANI/GO_x-TES engendered enzymatic reactions producing H_2O_2, wherein the ensuing unstable H_2O_2 underwent decomposition to yield H^+, inducing the protonation of PANI and engendering alterations in its conductivity and output values. Relative to pristine PANI/GO_x, NGQDs/PANI/GO_x-based TES exhibited superior sensitivity (23.52 mM^{-1}) in glucose detection attributable to improved electron transport and surface charge modulation by NGQDs (Fig. 8c), resulting in an enhanced voltage signals from 28 to 40 V upon increasing the glucose concentration from 0 to 2 mM (Fig. 8d). This highlighted the feasibility of wearable TES on human skin, showcasing their reliable and sensitive operation facilitated by a self-driving system obviating external power sources.

By incorporating different percentages of Prussian blue nanoparticles (PBNPs) in PEDOT:PSS, Xu *et al.*[112] develop a non-invasive hydrogel-based biosensor using capable of accurately measuring glucose levels in rabbit serum. In a hydrogel-based conductive biosensor, the hydrogel matrix serves as a scaffold for immobilizing bioreceptors, such as enzymes, antibodies, or DNA strands, which selectively bind to the target analyte. Here, the PBNPs were utilized for catalyzing H_2O_2, while PEDOT:PSS served as a conducting framework to facilitate swift electron transfer. The sensing performance was evaluated using chronoamperometry and CV in both rabbit serum and PBS, and was compared with that of a commercial glucometer. The 5% PBNPs-containing electrode demonstrated the highest sensitivity of 1474.0 μA mM^{-1} cm^{-2} towards 0.08 mM of glucose (Fig. 8e, pink bar), which is 11-fold higher than pure PB (129.0 μA mM^{-1} cm^{-2}, Fig. 8e, blue bar) and 2.7-fold higher than PEDOT:PSS/PB

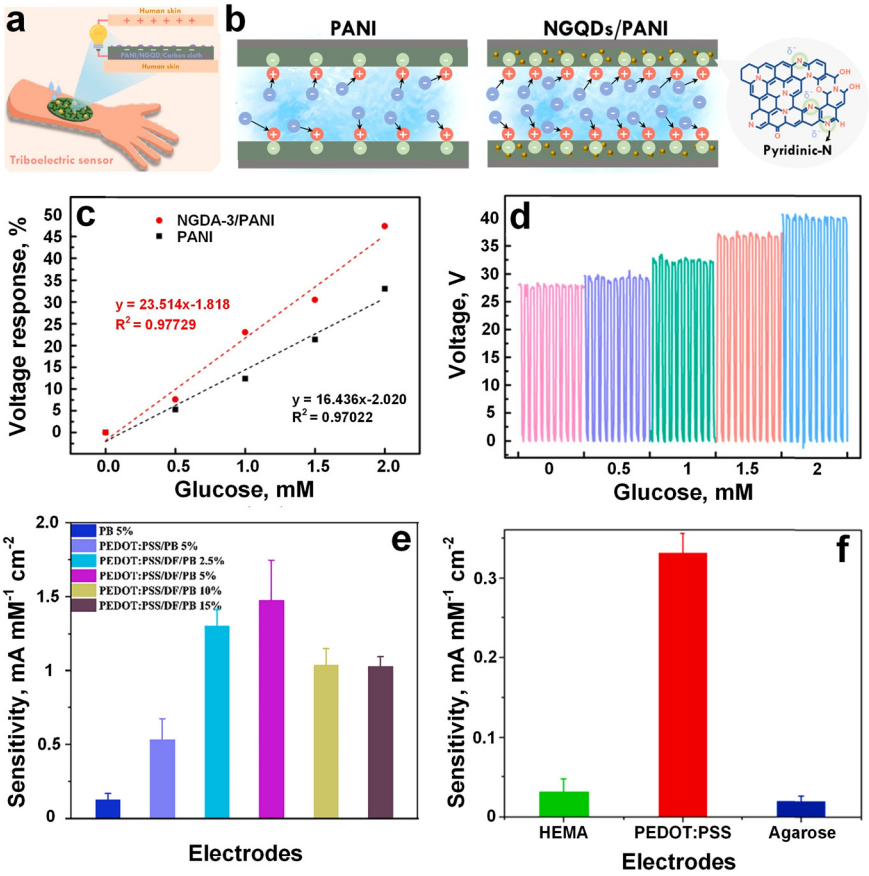

Fig. 8 a) Schematic illustration of wearable sweat test based on NGQDs/PANI. b) The working principle of zeta potential measurement for PANI and NGQDs/PANI thin films. c) Voltage response comparison of pristine PANI and NGQD-3/PANI/GO_x. d) Output voltage against different glucose concentration (adapted with permission from ref. 111 copyright 2023, Elsevier). e) Sensitivity against H_2O_2 of PBNPs containing electrode (5% PBNPs showed highest conductivity, green triangle, and 15% PBNPs showed lowest conductivity, brown triangle). f) The HEMA, EDPOD, and agarose containing different hydrogel sensor clips for glucose detection sensitivity (adapted with permission from ref. 112 copyright 2022, Elsevier).

without PBNPs (531.1 μA mM^{-1} cm^{-2}, Fig. 8e, purple bar). However, increasing PBNPs content up to 15% significantly reduced the sensitivity of the sensor down to 80 μA mM^{-1} cm^{-2} (Fig. 8e, brown bar), which could be attributed to hindered electronic transport on the electrode surface caused by the weak conductivity of PBNPs. Furthermore, the current density of the PEDOT:PSS-based sensor with non-conductive hydrogels (agarose and hydroxyethyl methacrylate (HEMA)-based hydrogels) resulted in a 10 times higher sensitivity of PEDOT:PSS-based sensor to glucose (330 μA mM^{-1} cm^{-2}) compared to HEMA (31.3 μA mM^{-1} cm^{-2}) and agarose hydrogel-modified electrodes (20.0 μA mM^{-1} cm^{-2}) (Fig. 8f).

In another approach, Çetin *et al.*[113] conducted a comprehensive investigation into the optimal enzyme concentration, comparing it to prior research focusing on either pre-functionalization of PAN nanofibers (NFs) with MWCNTs or post-functionalization with corresponding conductive polymers (*e.g.* PPy and PEDOT). The results highlighted enzyme concentration as a crucial factor in biosensor performance, with optimal concentrations found to be approximately 92.5 U for MWCNTs/PEDOT NFs and approximately 46.25 U for MWCNTs/PPy NFs. Higher enzyme concentrations (~255 U, ~370 U) were observed to diminish sensitivity and overall detection efficiency of the biosensing matrices. Incorporating MWCNTs into the NFs enhanced sensitivity and LOD, even at non-optimal enzyme concentrations, with the most significant improvement seen at the optimal concentration. PEDOT-based biosensors demonstrated slightly superior performance to PPy-based ones, both in the presence and absence of MWNCTs. The achieved analytical parameters are among the highest reported to date, with good stability, suggesting practical feasibility for detecting other analytes of interest.

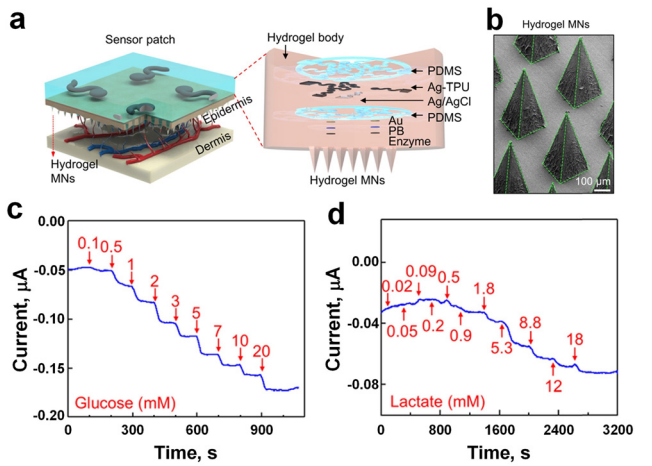

Fig. 9 a) Schematics and images of the sensor patch applied to the skin (left), and unassembled components (right). b) The SEM image displaying the hydrogel MNs. Benchtop evaluation: amperometric response of c) glucose, and d) lactate sensor patch (adapted with permission from ref. 118, copyright 2023, American Chemical Society).

Polymeric matrices

Polymeric materials are integral to the field of electrochemical sensor technology, functioning not only as electrodes but also as adaptable matrices. They provide a versatile platform for integrating different sensing elements, thereby improving the performance and stability of electrochemical sensors. Commonly employed polymeric matrices encompass hydrogels,[114–116] and elastomers,[107,117] each tailored to specific requirements in wearable sensing applications. Dai *et al.*[118] developed a wearable sensor patch (Fig. 9a) equipped with hydrogel MNs (Fig. 9b) for *in situ* analysis of interstitial fluid, particularly focusing on glucose and lactate monitoring. The MNs, made from methacrylated hyaluronic acid (MeHA), known for its exceptional swelling capacity and mechanical robustness,[119] were selected for their effectiveness in extracting ISF. The sensitivity of the sensor against glucose and lactate was evaluated using benchtop and *in vivo* assessment methods. In the benchtop method, the sensor exhibited rapid stabilization of the current signal within 60 seconds for glucose (Fig. 9c) and 120 seconds for lactate (Fig. 9d), and robust sensing performance against common interfering substances. Sensitivity analyses revealed *in vitro* sensitivities of 0.024 ± 0.002 μA mM^{-1} for glucose (Fig. 9c) and 0.0030 ± 0.0004 μA mM^{-1} for lactate (Fig. 9d), with linear ranges of 0.1–3 mM and 0.1–12 mM, respectively. For *in vivo* evaluation, the sensor's effectiveness was tested on mice, showing a sensitivity of 0.020 ± 0.001 μA mM^{-1} and a detection range of 1–8 mM for glucose sensing, holding a promise as a minimally invasive platform for continuous monitoring of multiple biomarkers in ISF, facilitating enhanced health monitoring and disease management.

Metal-based electrochemical sensors

Metallic-based electrochemical sensors have emerged as promising tools for sweat analysis, offering precise and sensitive detection of various biomarkers. These sensors utilize metallic materials (Au, Pt, Ag), as the working electrode,[120,121] capitalizing on their inherent conductivity and electrocatalytic properties. The rapid electron transfer kinetics facilitated by metallic substrates contribute to enhanced sensitivity and detection limits, making them ideal for analyzing sweat constituents such as glucose, lactate, and electrolytes.[47,55] Surface modifications with specific modifiers or nanostructures further refine selectivity and stability, ensuring accurate and reliable measurements. Such sensors hold great potential for non-invasive monitoring of physiological parameters through sweat analysis, paving the way for personalized healthcare and athletic performance optimization. Zhao *et al.*[47] developed a flexible nonenzymatic sweat glucose sensor based on Au nanoflowers (Au NFs) coated carbon cloth (CC) and gauze (Fig. 10a–c). The SEM image confirmed the outer surface of the WE (Au NFs) was coated by the CC (Fig. 10d). A chemical reduction method was applied to synthesize Au NFs on the surface of the CC and used Au NFs@CC as a WE for nonenzymatic glucose catalysis. Another CC was employed as a CE and RE. The

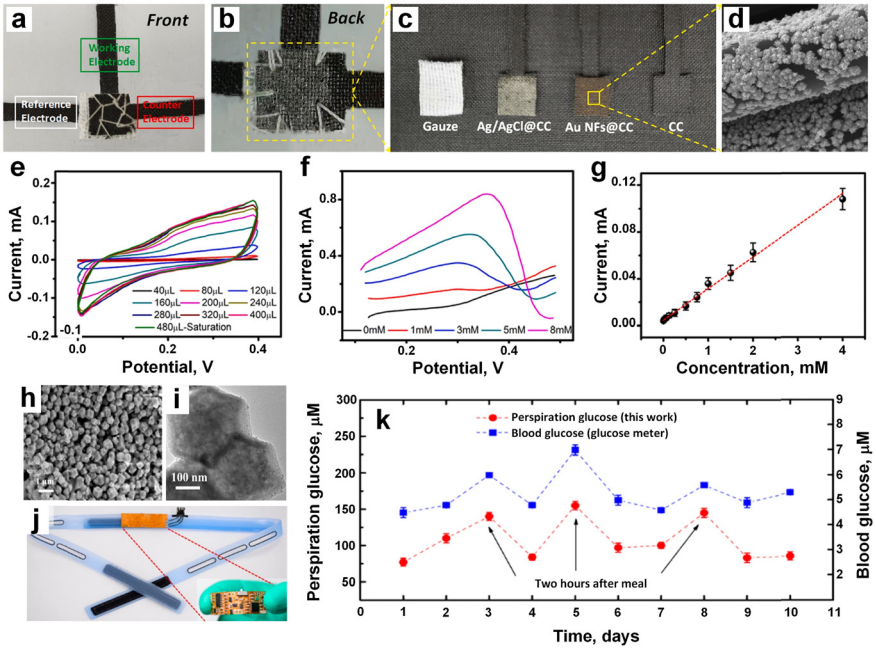

Fig. 10 a) The front and b) back side of the flexible sensor prepared by CC, and gauze. c) The disassembled of the all component of the sensor. d) The SEM image of the WE coated by CC. e) The electrode showed good conductivity against PBS solution, and 480 μL solution showed highest conductivity. f) The LVS analysis with different glucose concentrations. g) The linear fitting cure current *vs.* concentration (adapted with permission from ref. 47, copyright 2024, Royal Society of Chemistry). h and i) The TEM observation of the encapsulated Pd NPs in ZIF-67. j) The electrode embedded within the sweatband. k) The glucose monitoring result in blood (blue), and sweat (red) (adapted with permission from ref. 122, copyright 2019, American Chemical Society).

wearable sweat glucose sensor was integrated by sewing three electrodes and two gauzes together (Fig. 10a). A low current was observed with 80 μL of PBS solution due to insufficient coverage of the WE surface, whereas 240 μL of PBS solution demonstrated good conductivity, and saturation occurred at 480 μL (Fig. 10e). LSV analysis with varying glucose concentrations (0, 1, 3, 5, and 8 mM) showed the sensor's ability to respond to different glucose levels (Fig. 10f). Amperometry was employed to assess the current response characteristics of the flexible sensor, revealing higher current flow with increased glucose concentration. Dilution of the solution resulted in reduced response current intensity. The sensor exhibited excellent current response characteristics for glucose determination, with calibrated parameters including sensitivity, linear interval, and stabilization time. The linear fitting curve showed linearity in the concentration range of 8.0–4.0 × 10^3 μM, with a calculated sensitivity of 63.9 μA mM^{-1} cm^{-2} and a limit of detection of 5.18 μM (Fig. 10g).

Zhu *et al.*[122] engineered a wearable perspiration glucose sensor featuring palladium nanoparticles (Pd NPs) encapsulated within a cobalt-based zeolitic imidazolate framework (ZIF-67) as the electrocatalyst. The device comprised three electrodes: the working electrode, fabricated from Pd@ZIF-67 (Fig. 10h and i), was screen-printed onto a PET film, while the counter electrode was prepared using carbon conductive ink similarly applied to the film. The RE entailed coating a composite membrane, containing polymer and electrolyte, onto an Ag/AgCl electrode. Integrating a nonenzymatic sensor with a flexible printed circuit board (FPCB) enabled Bluetooth connectivity to an Android-based smartphone app, seamlessly embedded within a sweatband for real-time perspiration glucose analysis (Fig. 10j). Glucose monitoring results in blood and sweat over a 10 day period (Fig. 10k). Using a commercial glucose meter for blood glucose assessment and the sweatband sensor for perspiration glucose examination, tests conducted on days 3, 5, and 8 intentionally followed meals by two hours. Remarkably, a robust correlation between blood glucose concentration (Fig. 10k, blue, right *y*-axis) and sweat glucose concentration (Fig. 10k, red, left *y*-axis) was observed, with a correlation factor approximating 0.2.

Padmanathan *et al.*[123] reported the synthesis of $Ni_3(PO_4)_2{\cdot}8H_2O$ nano/microflakes on nickel foam (NF) using a facile one-pot hydrothermal method and explored its multifaceted utility. The fabricated electrode demonstrates impressive performance across various domains, notably as a sensor for monitoring glucose and pH levels in sweat and as a constituent in a hybrid energy-storage device. Exhibiting a specific capacity of 301.8 mAh g^{-1} (1552 F g^{-1}) at a current density of 5 mA cm^{-2}, the electrode maintains 84% of its initial capacity after 10 000 cycles. Additionally, when integrated with activated carbon as the negative electrode, the resulting supercapattery comprising $Ni_3(PO_4)_2{\cdot}8H_2O$/NF manifests a high specific energy of 33.4 W h kg^{-1} accompanied by a power density of 165.5 W kg^{-1}. Functioning as an electrocatalyst for nonenzymatic glucose sensing,

$Ni_3(PO_4)_2{\cdot}8H_2O$/NF exhibits exceptional sensitivity (24.39 mA mM^{-1} cm^{-2}) along with a low detection limit of 97 nM (S/N = 3). Furthermore, as a pH sensor for sweat, the electrode offers precise detection capabilities across the pH range of 4 to 7. Owing to its remarkable electrochemical attributes, this three-dimensional nanoporous $Ni_3(PO_4)_2{\cdot}8H_2O$/NF electrode emerges as a promising candidate for diverse applications in electrochemical energy storage and biosensing.

Chen *et al.*[55] developed a pinecone-shaped glucose biosensor, made of electrodeposited nano-pinecone structure (approximately 600 nm in size) on stainless-steel acupuncture needle (AN), using a composite microelectrode of Au and nickel (Ni) nanoparticles (Fig. 11a–c). Upon contact with glucose, the surface of the electrode facilitated the conversion of glucose molecules to gluconolactone. Fig. 11d demonstrates that as glucose concentration gradually increased, the peak of anodic current also increased, while the peak of cathodic currents declined, indicating strong electrocatalytic capacity for glucose oxidation in an alkaline environment by Ni/Au/AN. Continuous addition of glucose into 0.1 M NaOH exhibited a step shape and stepwise graph increase in response current, indicating a proportional response to glucose addition (Fig. 11e). Comparative analysis revealed that the Ni/Au/AN composite also exhibited an exceptional amperometric response at low glucose concentration (Fig. 11f) and significantly enhanced electrocatalytic activity, featuring an extended linear range, heightened sensitivity and a reduced LOD in contrast to Ni/AN or Au/AN electrode. Notably, the presence of a matrix of AuNPs significantly enhanced the electrochemical response of NiNPs for glucose detection, potentially attributed to the abundance of active sites within the bimetallic hierarchy. Under optimized conditions, the nonenzymatic biosensor demonstrated dual linear relationships, boasting sensitivities of 766.02 and 368.77 (μA mM^{-1} cm^{-2}) and a LOD of 0.14 μM. Operating within a concentration range of 0.5 μM to 1.5 mM and 1.5–5 mM (Fig. 11g), the Ni/Au/AN biosensor exhibited exceptional selectivity, stability, and repeatability surpassing previous electrode configurations. The developed biosensor presents a

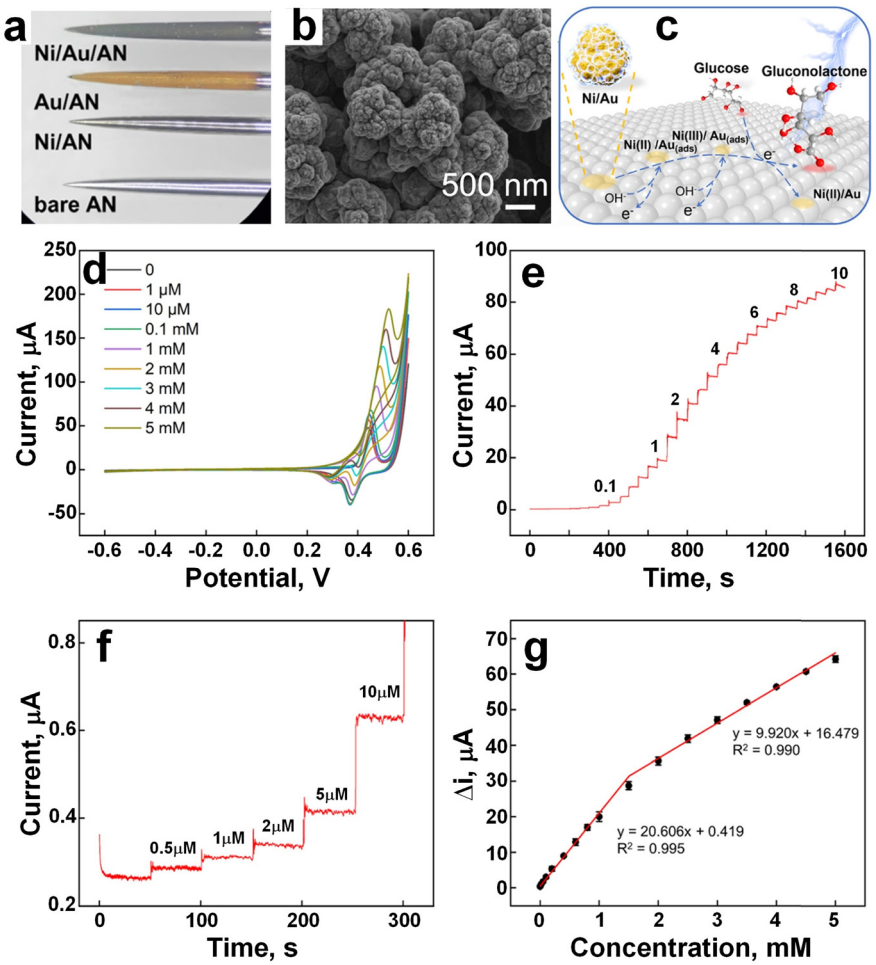

Fig. 11 a) The images of AN, Au/AN, Ni/AN, and Ni/Au/AN under bright-field. b) SEM image of the Ni/Au/AN. c) The conversion of the glucose molecule to gluconolactone. d) The conductivity of the electrode increased with gradually increasing the glucose concentration in 0.1 M NaOH. e) Stepwise increasing of the current upon addition of the glucose in 0.1 M NaOH. f) Stepwise increasing of the current at low glucose concentration in 0.1 M NaOH. g) The linearity curve between current response and glucose concentrations (adapted with permission from ref. 55, copyright 2022, American Chemical Society).

promising avenue for point-of-care clinical monitoring, offering effective detection of glucose levels in human serum.

A dual-structural Pt–Ni hydrogel with interconnected networks of PtNi nanowires and $Ni(OH)_2$ nanosheets were engineered by Li *et al.*[124] exhibiting excellent electrocatalytic activity and stability in glucose oxidation under neutral conditions. Specifically, the PtNi (1 : 3) dual hydrogel shows significantly higher activity in glucose electro-oxidation compared to pure Pt and Ni hydrogels. This enhanced activity, combined with structural stability, flexibility, and self-healing properties, enables the development of a high-performance non-enzymatic glucose sensing chip. The chip demonstrates high sensitivity, excellent selectivity, flexibility, and outstanding long-term stability, lasting over 2 months.[124] It maintains consistent performance even under mechanical deformation (0 to 90°), with a deviation of <1.84%.[125] In another approach, an on-chip disposable nano-biosensor[126] was fabricated to facilitate a painless testing approach with sufficient sensitivity to saliva glucose levels. The WE was functionalized by incorporating SWNTs, multilayers of chitosan (CS), Au nanoparticles, and GO_x. The CS–AuNP–GO_x unit was repeatedly coated to form a multilayer, with layer adjustments made to optimize sensing performance. After saliva absorption using a dental cotton roll, large molecules were filtered out using a polyvinylidene fluoride (PVDF) membrane, and the membrane was fixed and stabilized with iron wire gauze. The collected samples were divided into two parts, with one part used for rapid glucose level identification using the sensor, while the other part was processed, centrifuged, and analyzed using a UV spectrophotometer to evaluate sensor accuracy. Clinical findings from glucose monitoring in healthy young adults revealed timely salivary glucose response post-meal ingestion compared to blood glucose, with exercise after meals resulting in decreased salivary and blood glucose concentrations. The sensor offers a convenient and painless means to determine blood glucose equivalents through salivary glucose monitoring, promising an alternative for diabetic patients.

Metal oxide-based electrochemical sensors

Metal oxide-based electrochemical sensors are cutting-edge technologies offering a non-invasive and convenient approach to monitor biomarkers for health and performance assessment.[22,127] These sensors pull the unique properties of metal oxides to detect specific analytes within sweat samples, enabling real-time monitoring of physiological parameters such as electrolytes, metabolites, and biomarkers.[128] Their sensitivity, selectivity, and low-cost fabrication make them attractive candidates for wearable devices aimed at personalized healthcare monitoring and fitness tracking.[21,23,129] This introduction explores the principles behind metal oxide-based electrochemical sensors and their applications in sweat analysis for various healthcare and performance-related purposes. Li *et al.*[130] developed a

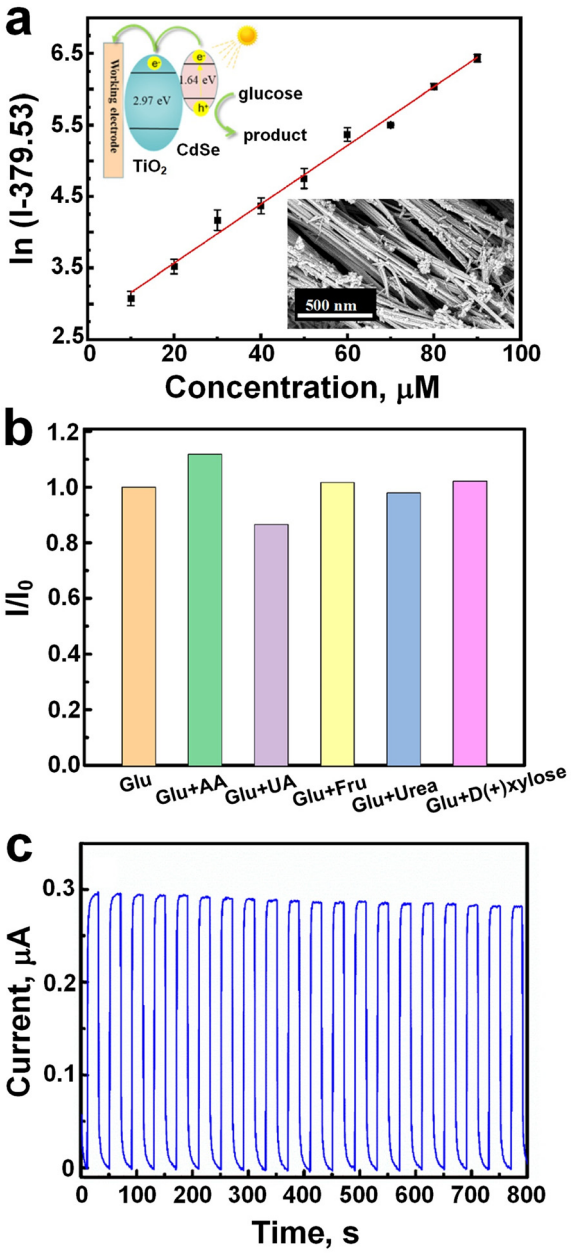

Fig. 12 a) The linearity curve for precise glucose detection between 90 to 10 μM concentration. b) Glucose sensing selectivity against different interfering species like ascorbic acid, uric acid, urea, fructose, and D-(+)-xylose. c) Photocurrent stability, and showed no significant change over 800 s (adapted with permission from ref. 130, copyright 2023, American Chemical Society).

cadmium selenide/titanium dioxide nanotube ($CdSe/TiO_2$-NTs) heterojunction as nonenzymatic photoelectrochemical sensor for precise glucose detection from 90 down to 10 μM (Fig. 12a). Using TiO_2 nanotubes as photoelectrodes, the fabricated sensor demonstrated a LOD of 3.1 μM for glucose detection (Fig. 12a), with excellent selectivity against interfering species such as ascorbic acid, uric acid, urea, fructose, and D-(+)-xylose (Fig. 12b). Furthermore, the sensor exhibited remarkable stability under continuous light

illumination, showing no significant photocurrent change over 800 s (Fig. 12c). Comparative analysis revealed superior performance of the CdSe/TiO_2NTs sensor in terms of lower LOD and enhanced stability compared to similar sensors,[131,132] establishing its reliability for glucose analysis in serum samples.

In another approach, Jiang *et al.*[133] have developed an enzyme-free smart sensor utilizing facet-dependent cuprous oxide (Cu_2O) for both enzyme-free glucose sensing and self-powered biofuel cell applications, marking a significant stride in sensor technology and biomedical applications. The team achieved the development of three distinct morphologies of Cu_2O-octahedral (Fig. 13a), cuboctahedral (Fig. 13b), and extended hexapod (Fig. 13c) nanostructures, by adjusting the ratio of ($CuCl_2$/NaOH/SDS) : NH_3OHCl from 1 : 3 to 1 : 2 and 1 : 1, respectively. Each of these Cu_2O morphologies exhibited sensitivity towards glucose detection, with initial oxidation potentials of 0.4, 0.3, and 0.4 V for the octahedral, cuboctahedral, and extended hexapod Cu_2O electrodes, respectively. Notably, the response signals of Cu_2O towards glucose surpassed those of interfering analytes such as K^+, Na^+, lactate, alanine, ascorbic acid, and uric acid. Integrated with wireless technology, the device enabled remote real-time detection of signals *via* a smartphone (Fig. 13d).

Similar to the conventional three-electrode system, the device showcased the process of glucose biosensing with oxidation peaks observed at 0.5–0.6 V in CV curves and a linear range of 0–4 mM in amperometric curves (Fig. 13e and f), indicating its potential practical application for wearable biosensing. Moreover, a wearable self-powered biofuel cell was designed, consisting of Cu_2O as the anode, Pt as the cathode, and sodium polyacrylate as the electrolyte, forming a sandwich structure on a carbon cloth platform (Fig. 13g). The anode facilitated the conversion circulation of Cu^{2+} to Cu^{3+}, serving as an efficient electron transfer mediator for oxidizing glucose molecules (Fig. 13g). Simultaneously, the cathode, rich in oxygen, composed of poly (trifluorovinyl chloride) as an internal oxygen reservoir, and Pt catalysts facilitated oxygen reduction, demonstrating its glucose-sensing capabilities through both open-circuit potential and power output. The signal response exhibited linearity with increasing glucose concentration within the range of 0–6 mM, with maximum power values reaching 1.4 μW at 6 mM (Fig. 13h and i). Beyond glucose monitoring, this newly designed enzyme-free wearable smart biosensing concept could seamlessly extend to the monitoring of clinical metabolites worn on the skin, offering significant opportunities for applications in early medical diagnosis, ongoing self-care for chronic conditions, and broader healthcare fields.

Very recently, Gopal *et al.*[134] made a breakthrough in material synthesis by creating a novel MXene-embedded porous activated carbon (AC)-based Cu_2O nanocomposite

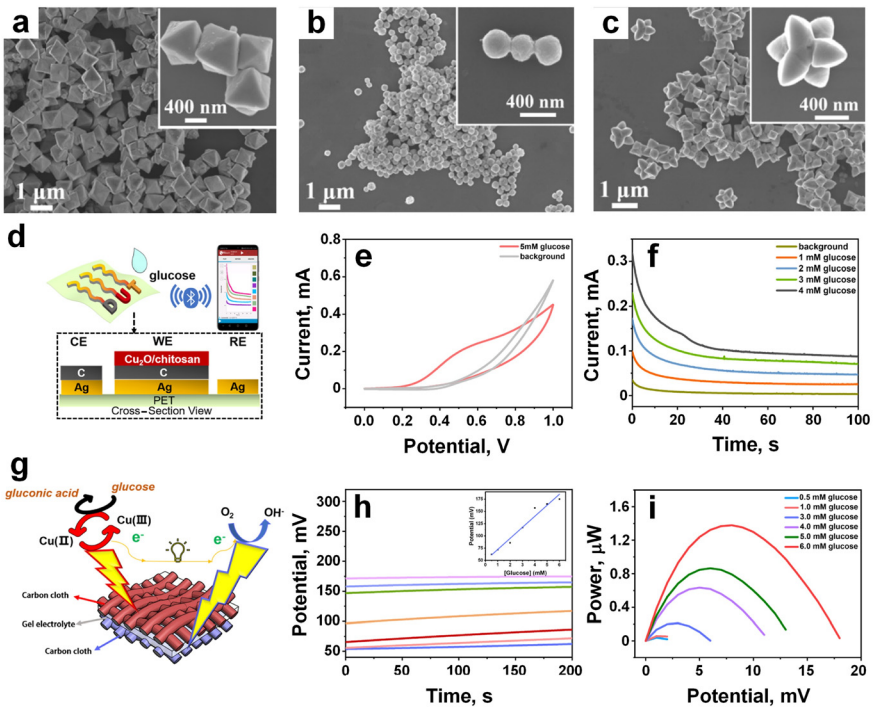

Fig. 13 a–c) The SEM image of the three types of Cu_2O materials (octahedral, cuboctahedral, and extended hexapod nanostructures), respectively. d) Integration wireless technology with the sensor for real time glucose monitoring. e) CV curves of cuboctahedral Cu_2O-based glucose sensor. f) Amperometric measurements of cuboctahedral Cu_2O-based glucose sensor. g) Schematic diagram of forming sandwich structure on the carbon cloth platform, and upon contact glucose molecule convert into gluconic acid. h) Potential measurement, and inset was linear curve. i) Power output performance against different glucose concentrations (adapted with permission from ref. 133, copyright 2021, American Chemical Society).

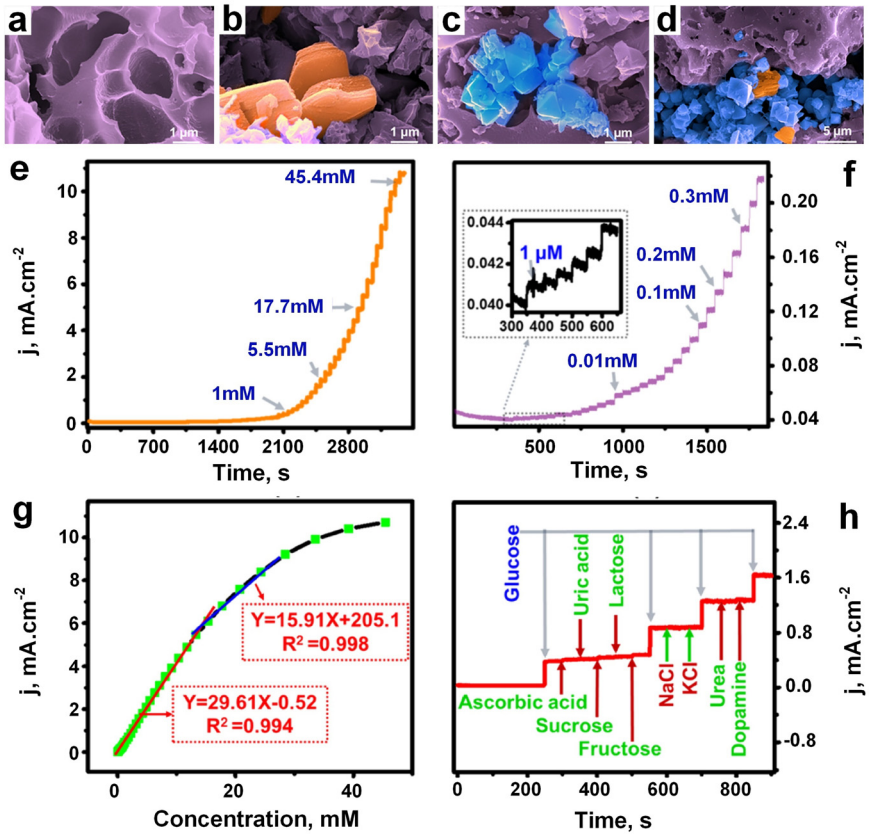

Fig. 14 FESEM images of a) activated carbon, b) M–AC composite, c) AC–Cu_2O composite and d) Cu_2O/M/AC composite. e) Amperometric response of Cu_2O/M/AC against different glucose concentrations. f) Amperometric response of Cu_2O/M/AC against different low concentration glucose solutions, and inset indicates response started from 1 μM concentration. g) Linearity curve. h) Glucose sensitivity after addition different interference substances like ascorbic acid, sucrose, fructose, urea, dopamine, uric acid, lactose, NaCl, and KCl (adapted with permission from ref. 134, copyright 2024, American Chemical Society).

(Cu_2O/M/AC) using the coprecipitation method. This innovative composite was then employed as a sensor probe for glucose detection, marking a significant advancement in sensor technology. During the synthesis process, when the activated carbon (Fig. 14a) and MXene were sonicated, accordion-like MXene sheets were effectively embedded in the pores of activated carbon, as depicted in Fig. 14b. This unique configuration was anticipated to enhance the electron transfer rate during the oxidation of glucose, a crucial aspect for sensor performance. Cu_2O nanoparticles (Fig. 14c) were then incorporated into the M/AC composite (Fig. 14d) *via* the coprecipitation method. The addition of MXene and Cu_2O had a substantial impact on the sensing parameters, as demonstrated through various electrochemical techniques such as CV, electrochemical impedance spectroscopy, and amperometric analysis.

To evaluate the performance of the Cu_2O/M/AC composite, amperometric measurements were conducted with the successive addition of glucose at increasing concentrations under stirring conditions, as shown in Fig. 14e. The composite exhibited a response starting from a glucose concentration of 1 μM (Fig. 14f). Impressively, it displayed two distinct linear ranges for glucose detection, with a LOD as low as 1.96 μM (Fig. 14g). The corresponding regression equations and sensitivity values were derived from the calibration curves, showcasing the composite's robust sensing capabilities. Furthermore, the Cu_2O/M/AC composite was tested in the presence of various components commonly found in blood composition, such as ascorbic acid, sucrose, fructose, lactose, uric acid, NaCl, KCl, urea, and dopamine. Encouragingly, these components did not interfere with the glucose sensitivity of the composite, as illustrated in Fig. 14h. These findings highlight the immense potential of the synthesized Cu_2O/M/AC nanocomposite as a versatile sensing material, particularly in the development of non-enzymatic glucose sensors. This breakthrough represents a significant step forward in sensor technology, promising enhanced accuracy and reliability in glucose monitoring and potentially other biomedical applications.

Other body fluid-based glucose monitoring technologies

Several studies have established a correlation between various characteristics of body fluids (blood, tear, saliva, urine, *etc.*)—such as conductivity, permittivity, dielectric

constant, blood refractive index, light scattering coefficient, bioimpedance, loss tangent, and permittivity—and glucose concentrations, allowing for non-invasive measurement.[18,19,21–23,135] Dervisevic *et al.*[136] pioneered the development of a high-density silicon-based microneedle (MN) array patch, boasting 9500 microneedles per square centimetre, for ISF glucose monitoring. Their approach involved sensor modification through covalent immobilization of glucose oxidase (GO_x) and bioconjugation strategies. This MN patch exhibited exceptional selectivity and sensitivity in detecting glucose within the physiological range. *In vivo* experiments involving ISF sensing in mice further demonstrated a robust correlation with blood glucose levels. In a separate study, Chang *et al.*[137] engineered a Nafion-coated flexible electrochemical sensor patch affixed to a watchband to extract ISF from the wrist. Clinical testing involving 23 volunteers revealed an 84.34% clinical accuracy in blood glucose measurements, indicating potential for refinement towards commercial viability.

Gomes *et al.*[138] introduced a flexible, bifunctional sensing platform using biodegradable mats for glucose detection in urine. This device successfully detected hydrogen peroxide (H_2O_2) in synthetic and human urine at low applied potentials (0 V *vs.* Ag/AgCl), with a detection range of 1.0 to 6.0 mM and a detection limit of 0.197 mM, while remaining free from interference. In another study, Davies *et al.*[139] employed a single-flash UV dual photopolymerization technique to fabricate a stable, nanoparticle-free, and reusable hydrogel-based holographic glucose sensor capable of continuous and quantitative monitoring of glucose levels in urine. This sensor exhibited high sensitivity and a low limit of detection for glucose in urine (0.06 mmol L^{-1}). However, urine glucose levels lack real-time correspondence with current blood glucose levels due to the time lag between changes in blood glucose and the appearance of glucose in urine, rendering it inadequate for monitoring rapid fluctuations in glucose levels. Furthermore, factors such as hydration status, kidney function, urinary glucose excretion, medications, diet, and renal threshold changes can introduce inaccuracies in urine glucose measurements.

In 2014, Google and Novartis introduced the concept of smart contact lenses for continuous monitoring of tear glucose levels. However, by 2018, the project was discontinued due to challenges in establishing a reliable correlation between tear glucose levels and blood glucose levels. Park *et al.*[140] developed a smart contact lens featuring an integrated LED display that deactivates when tear glucose levels surpass a threshold of 0.9 mM, offering a convenient real-time glucose sensing capability. Safety considerations remain paramount, necessitating thorough assessment of device toxicity in human subjects, given that most advancements have primarily been evaluated in animal models. Optical transparency and mechanical stretchability are crucial attributes for wearable contact lenses, yet comprehensive data on these properties are currently limited in the literature. Power supply remains an ongoing challenge, as many devices still rely on external sources, although biofuel cells show promise for self-powered contact lenses, albeit with validation only *in vitro* thus far. Despite the increasing sophistication of these devices over time, there remains substantial scope for innovation and enhancement.

Among various biofluids, saliva has garnered interest for non-invasive glucose monitoring due to its larger sample volumes compared to fluids like ISF or blood, despite typically lower glucose concentrations. Arakawa *et al.*[141] designed a wearable mouthguard biosensor coated with cellulose acetate for *in vivo* salivary glucose measurement. This sensor exhibited a glucose concentration range of 1.75–10 000 μmol L^{-1}, encompassing typical salivary sugar concentrations of 20–200 μmol L^{-1}. Garcia-Carmona *et al.*[142] developed a non-invasive saliva biomarker monitoring device tailored for infant saliva. They integrated all components into a pacifier, leveraging the infant's mouth movements to facilitate efficient saliva pumping and unidirectional flow into the electrochemical chamber, enabling seamless biomarker monitoring.

Summary and outlook

The evolution of electrochemical glucose sensors has witnessed substantial strides in accuracy and reliability. Initial iterations encountered hurdles related to calibration, interference, and sensor drift. These sensing technologies rely on diverse materials to optimize sensing processes and enhance sensor performance. The choice of materials significantly influences sensor sensitivity, selectivity, and stability. Carbon-based electrochemical sensors typically employ CNTs such as SWCNTs, DWCNTs, and MWCNTs, alongside graphene and carbon quantum dots. These nanostructures contribute to chemical and thermal stability while boosting sensor sensitivity to glucose. Additionally, combining AuNS with carbon materials enhances sensor stretchability. MOFs are emerging as promising materials for wearable sensors, enabling continuous and accurate blood glucose monitoring in sweat. Notably, different MOF-based electrochemical sensors like NCGP, NCMP, and GO_x–GA–Ni/Cu-MOFs exhibit varying sensitivities, highlighting their potential in glucose sensing. Polymeric-based electrochemical sensors have gained traction due to their versatility and inherent properties suitable for sensing applications. Conductive polymers like PANI are common in sweat glucose monitoring devices, while polymeric matrices like MeHA MNs demonstrate exceptional swelling capacity and mechanical robustness, facilitating interstitial fluid extraction. Metals such as Au, Pt, Pd, Co, and Ag serve as effective working electrodes, with nanostructured materials like Pd@ZIF-67 and $Ni_3(PO_4)_2{\cdot}8H_2O$ demonstrating high glucose sensitivity. Metal oxide-based sensors like CdSe/TiO_2 NTs, and Cu_2O/M/AC also exhibit high detection limits without interference from other analytes like ions and organic compounds.

Ongoing research aims to refine sensor designs, optimize calibration algorithms, and mitigate external factors affecting

accuracy, thereby ensuring users can rely on these devices for precise glucose monitoring. Artificial intelligence-driven early warning systems have the potential to alert users to impending hypoglycemic or hyperglycemic events, empowering them to maintain glucose within target ranges. Technological advancements are poised to refine predictive capabilities further. Despite substantial progress, challenges persist, necessitating attention in future research endeavors. One of the foremost challenges in wearable sweat glucose sensors is extending their operational lifespan. Prolonging sensor longevity is crucial to reduce replacement frequency, enhancing user convenience and cost-effectiveness. Achieving this involves optimizing sensor materials for durability and resistance to degradation in the sweat environment. Research focuses on developing robust, biocompatible materials that maintain sensor performance despite harsh conditions. Advances in sensor encapsulation and protective coatings further aim to increase resistance to wear and corrosion, extending sensor lifespan. Another critical challenge is reducing the need for frequent sensor recalibration. While calibration is vital for accurate measurements, frequent recalibrations can be inconvenient and introduce variability. Innovative approaches include developing self-calibrating sensors capable of continuous glucose monitoring without manual adjustments. This entails utilizing advanced algorithms for real-time data processing and signal correction, integrating internal reference electrodes, and improving sensor stability to minimize drift over time. Enhancing sensor stability reduces the frequency of recalibration, ensuring consistent and reliable glucose monitoring for users.

The future trajectory of wearable glucose sensors entails exploring novel sensing modalities beyond traditional electrochemical methods. Advanced technologies, such as non-invasive or minimally invasive glucose monitoring, hold promise for enhancing user experience and extending continuous monitoring to a broader demographic. Interoperability remains a crucial aspect, with integration efforts across health monitoring devices and healthcare systems facilitating holistic health monitoring. Standardization initiatives in data formats and communication protocols will expedite seamless data exchange, fostering collaborative diabetes management approaches.

Conflicts of interest

The author declares no conflict of interest.

Acknowledgements

N. N. acknowledges the financial support received from Cochlear – Macquarie University Joint Fund and the Cancer Institute New South Wales (NSW) Research Fellowship (2022/ECF1417). H. R. acknowledges the financial support received from Japanese Government (MEXT) Scholarship.

References

1 S. Ashrafzadeh and O. Hamdy, *Cell Metab.*, 2019, **29**, 564–575.
2 G. E. Umpierrez and B. P. Kovatchev, *Am. J. Med. Sci.*, 2018, **356**, 518–527.
3 D. Rodbard, *Diabetes Technol. Ther.*, 2017, **19**, S-25–S-37.
4 J. Kim, J. R. Sempionatto, S. Imani, M. C. Hartel, A. Barfidokht, G. Tang, A. S. Campbell, P. P. Mercier and J. Wang, *Adv. Sci*, 2018, **5**, 1800880.
5 H. Park, W. Park and C. H. Lee, *NPG Asia Mater.*, 2021, **13**, 23.
6 A. Sharma, A. Singh, V. Gupta and S. Arya, *Sens. Diagn.*, 2022, **1**, 387–404.
7 A. Mishra, P. K. Singh, N. Chauhan, S. Roy, A. Tiwari, S. Gupta, A. Tiwari, S. Patra, T. R. Das, P. Mishra and A. S. Nejad, *Sens. Diagn.*, 2024, DOI: **10.1039/D4SD00017J**.
8 P. Bhardwaj, B. Arora, S. Saxena, S. Singh, P. Palkar, J. S. Goda and R. Banerjee, *Sens. Diagn.*, 2024, **3**, 504–535.
9 S. Roy, F. Arshad, S. Eissa, M. Safavieh, S. G. Alattas, M. U. Ahmed and M. Zourob, *Sens. Diagn.*, 2022, **1**, 87–105.
10 M. Shang, J. Guo and J. Guo, *Sens. Diagn.*, 2023, **2**, 1123–1144.
11 R. D. Crapnell, A. Garcia-Miranda Ferrari, N. C. Dempsey and C. E. Banks, *Sens. Diagn.*, 2022, **1**, 405–428.
12 G. Manasa, R. J. Mascarenhas, N. P. Shetti, S. J. Malode, A. Mishra, S. Basu and T. M. Aminabhavi, *ACS Appl. Bio Mater.*, 2022, **5**, 945–970.
13 V. M. Regufe, C. M. Pinto and P. M. Perez, *Porto Biomed. J.*, 2020, **5**, e101.
14 R. M. Bergenstal, B. W. Bode, A. Bhargava, Q. Wang, A. W. Knights and A. M. Chang, *Diabetes Ther.*, 2023, **14**, 1933–1945.
15 A. L. Burrack, T. Martinov and B. T. Fife, *Front. Endocrinol.*, 2017, **8**, 317011.
16 C. M. Rotella, L. Pala and E. Mannucci, *Int. J. Endocrinol. Metab.*, 2013, **11**, 137.
17 W. H. Organization, *Global status report on noncommunicable diseases*, World Health Organization, 2014.
18 N. Nasiri and C. Clarke, *Sensors*, 2019, **19**, 462.
19 N. Nasiri and C. Clarke, *Biosensors*, 2019, **9**, 43.
20 X. Chen, M. Leishman, D. Bagnall and N. Nasiri, *Nanomaterials*, 2021, **11**, 1927.
21 N. Nasiri and A. Tricoli, in *Wearable Technologies*, IntechOpen, 2018.
22 N. Nasiri, *Wearable Devices—Big Wave Innovation*, 2019.
23 A. Tricoli, N. Nasiri and S. De, *Adv. Funct. Mater.*, 2017, **27**, 1605271.
24 F. Gao, C. Liu, L. Zhang, T. Liu, Z. Wang, Z. Song, H. Cai, Z. Fang, J. Chen and J. Wang, *Microsyst. Nanoeng.*, 2023, **9**, 1–21.
25 M. Bariya, H. Y. Y. Nyein and A. Javey, *Nat. Electron.*, 2018, **1**, 160–171.
26 Y. Song, D. Mukasa, H. Zhang and W. Gao, *Acc. Mater. Res.*, 2021, **2**, 184–197.

27 Z. Lou, L. Li, L. Wang and G. Shen, *Small*, 2017, **13**, 1701791.
28 S. N. Toala, Z. Sun, Y. Yue, S. F. Gonski and W.-J. Cai, *Sens. Diagn.*, 2024, **3**, 599–622.
29 M. Cuartero, M. Parrilla and G. A. Crespo, *Sensors*, 2019, **19**, 363.
30 E. Verrinder, K. K. Leung, M. K. Erdal, L. Sepunaru and K. W. Plaxco, *Sens. Diagn.*, 2024, **3**, 95–103.
31 N. Coppedè, M. Giannetto, M. Villani, V. Lucchini, E. Battista, M. Careri and A. Zappettini, *Org. Electron.*, 2020, **78**, 105579.
32 Q. Chen, Y. Liu, K. Gu, J. Yao, Z. Shao and X. Chen, *Biomacromolecules*, 2022, **23**, 3928–3935.
33 M. H. Hassan, C. Vyas, B. Grieve and P. Bartolo, *Sensors*, 2021, **21**, 4672.
34 J. Liu, J. Shen, S. Ji, Q. Zhang and W. Zhao, *Sens. Diagn.*, 2023, **2**, 36–45.
35 G. M. Duran, T. E. Benavidez, J. G. Giuliani, A. Rios and C. D. Garcia, *Sens. Actuators, B*, 2016, **227**, 626–633.
36 S. Campuzano, M. Pedrero, P. Yáñez-Sedeño and J. M. Pingarrón, *Sens. Actuators, B*, 2021, **345**, 130349.
37 E. Primiceri, M. S. Chiriacò, F. M. Notarangelo, A. Crocamo, D. Ardissino, M. Cereda, A. P. Bramanti, M. A. Bianchessi, G. Giannelli and G. Maruccio, *Sensors*, 2018, **18**, 3607.
38 H. Zafar, A. Channa, V. Jeoti and G. M. Stojanović, *Sensors*, 2022, **22**, 638.
39 L. C. Clark and C. Lyons, *Ann. N. Y. Acad. Sci.*, 1962, **102**, 29–45.
40 A. H. Kadish, *Am. J. Med. Electron.*, 1964, **3**, 82–86.
41 S. J. Updike and G. P. Hicks, *Nature*, 1967, **214**, 986–988.
42 J. S. Cheah and A. F. Wong, *Singapore Med. J.*, 1974, **15**(1), 51–52.
43 G. S. Wilson, Y. Zhang, G. Reach, D. Moatti-Sirat, V. Poitout, D. R. Thévenot, F. Lemonnier and J.-C. Klein, *Clin. Chem.*, 1992, **38**, 1613–1617.
44 M. A. Burns, B. N. Johnson, S. N. Brahmasandra, K. Handique, J. R. Webster, M. Krishnan, T. S. Sammarco, P. M. Man, D. Jones and D. Heldsinger, *Science*, 1998, **282**, 484–487.
45 J. M. Lee, E. Carlson, A. Albanese-O'Neill, C. Demeterco-Berggren, S. D. Corathers, F. Vendrame, R. S. Weinstock, P. Prahalad, G. T. Alonso and M. Kamboj, *Diabetes Technol. Ther.*, 2021, **23**, 642–651.
46 S. K. Garg and E. Rodriguez, *Diabetes Technol. Ther.*, 2022, **24**, S-2–S-20.
47 Z. Zhao, T. Wang, K. Li, D. Long, J. Zhao, F. Zhu and W. Gong, *Sens. Actuators, B*, 2023, **388**, 133798.
48 L. Yang, H. Wang, A. M. Abdullah, C. Meng, X. Chen, A. Feng and H. Cheng, *ACS Appl. Mater. Interfaces*, 2023, **15**, 34332–34342.
49 Y. Xia, T. Su, Z. Mi, Z. Feng, Y. Hong, X. Hu and Y. Shu, *Anal. Chim. Acta*, 2023, **1278**, 341754.
50 S. Das, B. Saha, M. Tiwari and D. K. Tiwari, *Sens. Diagn.*, 2023, **2**, 268–289.
51 S. Aghris, M. Azriouil, F. E. Ettadili, A. Loukili, F. Laghrib, A. Farahi, M. Bakasse, S. Lahrich and M. A. El Mhammedi, *Sens. Diagn.*, 2023, **2**, 398–408.
52 V. Mishyn, M. Aslan, A. Hugo, T. Rodrigues, H. Happy, R. Sanyal, W. Knoll, F. Baudoux, V. Bouchiat, R. O. Bilyy, R. Boukherroub, A. Sanyal and S. Szunerits, *Sens. Diagn.*, 2022, **1**, 739–749.
53 H. Wang, S. Li, H. Lu, M. Zhu, H. Liang, X. Wu and Y. Zhang, *Small Methods*, 2023, **7**, 2201340.
54 S. Kumar, H. K. Sidhu, A. K. Paul, N. Bhardwaj, N. S. Thakur and A. Deep, *Sens. Diagn.*, 2023, **2**, 1390–1413.
55 J. Chen, G. Liu, Q. Xiao, C. Wang, Z. Zhou, C. Gu, Z.-Z. Yin and H. Liu, *ACS Appl. Nano Mater.*, 2022, **5**, 13319–13331.
56 Y. Shu, T. Su, Q. Lu, Z. Shang, Q. Xu and X. Hu, *Anal. Chem.*, 2021, **93**, 16222–16230.
57 S. Ma, X. Yuan, X. Yin, Y. Yang and L. Ren, *Microchem. J.*, 2023, **195**, 109324.
58 L. Xu, X. Zhang, Z. Wang, A. A. Haidry, Z. Yao, E. Haque, Y. Wang, G. Li, T. Daeneke and C. F. McConville, *Nanoscale*, 2021, **13**, 11017–11040.
59 A. Khan, E. DeVoe and S. Andreescu, *Sens. Diagn.*, 2023, **2**, 529–558.
60 L. Wang, S. Xie, Z. Wang, F. Liu, Y. Yang, C. Tang, X. Wu, P. Liu, Y. Li and H. Saiyin, *Nat. Biomed. Eng.*, 2020, **4**, 159–171.
61 Q. Huang, X. Lin, L. Tong and Q.-X. Tong, *ACS Sustainable Chem. Eng.*, 2020, **8**, 1644–1650.
62 A. U. Alam and M. J. Deen, *Anal. Chem.*, 2020, **92**, 5532–5539.
63 A. A. Lahcen, S. Rauf, T. Beduk, C. Durmus, A. Aljedaibi, S. Timur, H. N. Alshareef, A. Amine, O. S. Wolfbeis and K. N. Salama, *Biosens. Bioelectron.*, 2020, **168**, 112565.
64 G. Balkourani, T. Damartzis, A. Brouzgou and P. Tsiakaras, *Sensors*, 2022, **22**, 355.
65 S. E. Elugoke, O. E. Fayemi, A. S. Adekunle, B. B. Mamba, T. T. Nkambule and E. E. Ebenso, *FlatChem*, 2022, **33**, 100372.
66 D. Rocco, V. G. Moldoveanu, M. Feroci, M. Bortolami and F. Vetica, *ChemElectroChem*, 2023, **10**, e202201104.
67 H. Habib, M. Alam, M. Aggarwal, I. S. Wani and S. Husain, in *Surface Modified Carbon Nanotubes: Fundamentals, Synthesis and Recent Trends*, ACS Publications, 2022, vol. 1, pp. 27–47.
68 M. M. Hassan, Y. Xu, M. Zareef, H. Li, Y. Rong and Q. Chen, *Crit. Rev. Food Sci. Nutr.*, 2023, **63**, 2851–2872.
69 C. J. Venegas, S. Bollo and P. Sierra-Rosales, *Micromachines*, 2023, **14**, 1752.
70 S. Y. Oh, S. Y. Hong, Y. R. Jeong, J. Yun, H. Park, S. W. Jin, G. Lee, J. H. Oh, H. Lee and S.-S. Lee, *ACS Appl. Mater. Interfaces*, 2018, **10**, 13729–13740.
71 E. Guzmán, F. Ortega and R. G. Rubio, *Energies*, 2022, **15**, 3399.
72 N. T. Garland, J. Schmieder, Z. T. Johnson, R. G. Hjort, B. Chen, C. Andersen, D. Sanborn, G. Kjeldgaard, C. C. Pola and J. Li, *ACS Appl. Mater. Interfaces*, 2023, **15**, 38201–38213.
73 R. Ye, D. K. James and J. M. Tour, *Adv. Mater.*, 2019, **31**, 1803621.
74 R. Ye, D. K. James and J. M. Tour, *Acc. Chem. Res.*, 2018, **51**, 1609–1620.

75 H. B. Wu and X. W. Lou, *Sci. Adv.*, 2017, **3**, eaap9252.
76 D. Liu, D. Zou, H. Zhu and J. Zhang, *Small*, 2018, **14**, 1801454.
77 M. Adeel, K. Asif, M. M. Rahman, S. Daniele, V. Canzonieri and F. Rizzolio, *Adv. Funct. Mater.*, 2021, **31**, 2106023.
78 B. Wang, Y. Luo, L. Gao, B. Liu and G. Duan, *Biosens. Bioelectron.*, 2021, **171**, 112736.
79 R. Ahmad, M.-S. Ahn and Y.-B. Hahn, *Electrochem. Commun.*, 2017, **77**, 107–111.
80 K. S. Bhat, R. Ahmad, J.-Y. Yoo and Y.-B. Hahn, *J. Colloid Interface Sci.*, 2017, **506**, 188–196.
81 R. Ahmad, N. Tripathy, J.-H. Park and Y.-B. Hahn, *Chem. Commun.*, 2015, **51**, 11968–11971.
82 G. Alberti, C. Zanoni, V. Losi, L. R. Magnaghi and R. Biesuz, *Chemosensors*, 2021, **9**, 108.
83 A. M. Sanjuán, J. A. R. Ruiz, F. C. García and J. M. García, *React. Funct. Polym.*, 2018, **133**, 103–125.
84 M. Pirzada and Z. Altintas, *Micromachines*, 2020, **11**, 356.
85 D. Vilela, A. Romeo and S. Sánchez, *Lab Chip*, 2016, **16**, 402–408.
86 A. Kaushik, R. Kumar, S. K. Arya, M. Nair, B. Malhotra and S. Bhansali, *Chem. Rev.*, 2015, **115**, 4571–4606.
87 P. Rebelo, E. Costa-Rama, I. Seguro, J. G. Pacheco, H. P. Nouws, M. N. D. Cordeiro and C. Delerue-Matos, *Biosens. Bioelectron.*, 2021, **172**, 112719.
88 Y. L. Liu, Z. H. Jin, Y. H. Liu, X. B. Hu, Y. Qin, J. Q. Xu, C. F. Fan and W. H. Huang, *Angew. Chem., Int. Ed.*, 2016, **55**, 4537–4541.
89 C. Zhang, H. Li, A. Huang, Q. Zhang, K. Rui, H. Lin, G. Sun, J. Zhu, H. Peng and W. Huang, *Small*, 2019, **15**, 1805493.
90 A. Economou, C. Kokkinos and M. Prodromidis, *Lab Chip*, 2018, **18**, 1812–1830.
91 J. Shi, S. Liu, L. Zhang, B. Yang, L. Shu, Y. Yang, M. Ren, Y. Wang, J. Chen and W. Chen, *Adv. Mater.*, 2020, **32**, 1901958.
92 M. Dulal, S. Afroj, J. Ahn, Y. Cho, C. Carr, I.-D. Kim and N. Karim, *ACS Nano*, 2022, **16**, 19755–19788.
93 W. He, C. Wang, H. Wang, M. Jian, W. Lu, X. Liang, X. Zhang, F. Yang and Y. Zhang, *Sci. Adv.*, 2019, **5**, eaax0649.
94 A. Hariharan, S. Kumar, M. Alagar, K. Dinakaran and K. Subramanian, *Polym. Bull.*, 2018, **75**, 93–107.
95 J. Huang, J. Wang, Z. Yang and S. Yang, *ACS Appl. Mater. Interfaces*, 2018, **10**, 8180–8189.
96 D. H. Lee, H. D. Yun, E. D. Jung, J. H. Chu, Y. S. Nam, S. Song, S.-H. Seok, M. H. Song and S.-Y. Kwon, *ACS Appl. Mater. Interfaces*, 2019, **11**, 21069–21077.
97 L. He, X. Zhou, W. Cai, Y. Xiao, F. Chu, X. Mu, X. Fu, Y. Hu and L. Song, *Composites, Part B*, 2020, **202**, 108446.
98 T. Allami, A. Alamiery, M. H. Nassir and A. H. Kadhum, *Polymer*, 2021, **13**, 2467.
99 L. Fu, A. Yu and G. Lai, *Chemosensors*, 2021, **9**, 282.
100 H. Shafique, J. de Vries, J. Strauss, A. Khorrami Jahromi, R. Siavash Moakhar and S. Mahshid, *Adv. Healthcare Mater.*, 2023, **12**, 2201501.
101 J. Y. Chen, P. Xie and Z. P. Zhang, *J. Chem. Eng.*, 2019, **361**, 615–624.
102 G. S. Geleta, Z. Zhao and Z. Wang, *Anal. Methods*, 2018, **10**, 4689–4694.
103 R. K. Pal, A. A. Farghaly, C. Wang, M. M. Collinson, S. C. Kundu and V. K. Yadavalli, *Biosens. Bioelectron.*, 2016, **81**, 294–302.
104 M. H. Naveen, N. G. Gurudatt and Y.-B. Shim, *Appl. Mater. Today*, 2017, **9**, 419–433.
105 Z. Xu, J. Song, B. Liu, S. Lv, F. Gao, X. Luo and P. Wang, *Sens. Actuators, B*, 2021, **348**, 130674.
106 T. Kaya, G. Liu, J. Ho, K. Yelamarthi, K. Miller, J. Edwards and A. Stannard, *Electroanalysis*, 2019, **31**, 411–421.
107 J. Lv, G. Thangavel, Y. Li, J. Xiong, D. Gao, J. Ciou, M. W. M. Tan, I. Aziz, S. Chen and J. Chen, *Sci. Adv.*, 2021, **7**, eabg8433.
108 Y.-C. Lin, M. Rinawati, L.-Y. Chang, Y.-X. Wang, Y.-T. Wu, Y.-H. Yen, K.-J. Chen, K.-C. Ho and M.-H. Yeh, *Sens. Actuators, B*, 2023, **383**, 133617.
109 F. Mazzara, B. Patella, C. D'Agostino, M. G. Bruno, S. Carbone, F. Lopresti, G. Aiello, C. Torino, A. Vilasi and A. O'Riordan, *Chemosensors*, 2021, **9**, 169.
110 T. Lim, Y. Kim, S.-M. Jeong, C.-H. Kim, S.-M. Kim, S. Y. Park, M.-H. Yoon and S. Ju, *Sci. Rep.*, 2019, **9**, 17294.
111 Y.-H. Chang, C.-C. Chang, L.-Y. Chang, P.-C. Wang, P. Kanokpaka and M.-H. Yeh, *Nano Energy*, 2023, **112**, 108505.
112 C. Xu, D. Jiang, Y. Ge, L. Huang, Y. Xiao, X. Ren, X. Liu, Q. Zhang and Y. Wang, *Chem. Eng. J.*, 2022, **431**, 134109.
113 M. Z. Çetin, N. Guven, R.-M. Apetrei and P. Camurlu, *Enzyme Microb. Technol.*, 2023, **164**, 110178.
114 S. Lin, B. Wang, Y. Zhao, R. Shih, X. Cheng, W. Yu, H. Hojaiji, H. Lin, C. Hoffman and D. Ly, *ACS Sens.*, 2019, **5**, 93–102.
115 P.-H. Lin, S.-C. Sheu, C.-W. Chen, S.-C. Huang and B.-R. Li, *Talanta*, 2022, **241**, 123187.
116 J. Wang, N. Zhang, Y. Tan, F. Fu, G. Liu, Y. Fang, X.-X. Zhang, M. Liu, Y. Cheng and J. Yu, *ACS Appl. Mater. Interfaces*, 2022, **14**, 21945–21953.
117 M. S. Brown, M. Mendoza, P. Chavoshnejad, M. J. Razavi, G. J. Mahler and A. Koh, *Adv. Mater. Technol.*, 2020, **5**, 2000242.
118 Y. Dai, J. Nolan, E. Madsen, M. Fratus, J. Lee, J. Zhang, J. Lim, S. Hong, M. A. Alam and J. C. Linnes, *ACS Appl. Mater. Interfaces*, 2023, **15**, 56760–56773.
119 B. Shriky, M. Babenko and B. R. Whiteside, *Gels*, 2023, **9**, 806.
120 Q. Zhai, L. W. Yap, R. Wang, S. Gong, Z. Guo, Y. Liu, Q. Lyu, J. Wang, G. P. Simon and W. Cheng, *Anal. Chem.*, 2020, **92**, 4647–4655.
121 S. Anastasova, B. Crewther, P. Bembnowicz, V. Curto, H. M. Ip, B. Rosa and G.-Z. Yang, *Biosens. Bioelectron.*, 2017, **93**, 139–145.
122 X. Zhu, S. Yuan, Y. Ju, J. Yang, C. Zhao and H. Liu, *Anal. Chem.*, 2019, **91**, 10764–10771.
123 N. Padmanathan, H. Shao and K. M. Razeeb, *ACS Appl. Mater. Interfaces*, 2018, **10**, 8599–8610.
124 G. Li, C. Wang, Y. Chen, F. Liu, H. Fan, B. Yao, J. Hao, Y. Yu and D. Wen, *Small*, 2023, **19**, 2206868.

125 G. Li, J. Hao, W. Li, F. Ma, T. Ma, W. Gao, Y. Yu and D. Wen, *Anal. Chem.*, 2021, **93**, 14068–14075.
126 W. Zhang, Y. Du and M. L. Wang, *Sens. Bio-Sens. Res.*, 2015, **4**, 23–29.
127 K. Mondal and A. Sharma, *RSC Adv.*, 2016, **6**, 94595–94616.
128 B. A. Hussein, A. A. Tsegaye, G. Shifera and A. M. Taddesse, *Sens. Diagn.*, 2023, **2**, 347–360.
129 L. Qian, A. R. Thiruppathi, J. van der Zalm and A. Chen, *ACS Appl. Nano Mater.*, 2021, **4**, 3696–3706.
130 Y.-L. Li, J. Tian, D.-J. Shi, J.-X. Dong, Z. Yue, G. Li, W.-P. Huang, S.-M. Zhang and B.-L. Zhu, *Langmuir*, 2023, **39**, 14935–14944.
131 R. Yuan, B. Yan, C. Lai, X. Wang, Y. Cao, J. Tu, Y. Li and Q. Wu, *ACS Omega*, 2023, **8**, 22099–22107.
132 L. Shangguan, C. Yan, H. Zhang, G. Xu, Y. Gao, Y. Li, D. Ge and J. Sun, *New J. Chem.*, 2022, **46**, 18680–18687.
133 Y. Jiang, T. Xia, L. Shen, J. Ma, H. Ma, T. Sun, F. Lv and N. Zhu, *ACS Catal.*, 2021, **11**, 2949–2955.
134 T. S. Gopal, J. T. James, B. Gunaseelan, K. Ramesh, V. Raghavan, K. Amarnath and V. Ganesh Kumar, *et al.*, *ACS Omega*, 2024, **9**(7), 8448.
135 N. Nasiri and A. Tricoli, in *21st Century Nanoscience–A Handbook*, CRC Press, 2020, pp. 1-1–1-17.
136 M. Dervisevic, M. Alba, L. Esser, N. Tabassum, B. Prieto-Simon and N. H. Voelcker, *ACS Appl. Mater. Interfaces*, 2021, **14**, 2401–2410.
137 T. Chang, H. Li, N. Zhang, X. Jiang, X. Yu, Q. Yang, Z. Jin, H. Meng and L. Chang, *Microsyst. Nanoeng.*, 2022, **8**, 25.
138 N. O. Gomes, R. T. Paschoalin, S. Bilatto, A. R. Sorigotti, C. S. Farinas, L. H. C. Mattoso, S. A. Machado, O. N. Oliveira Jr and P. A. Raymundo-Pereira, *ACS Sustainable Chem. Eng.*, 2023, **11**, 2209–2218.
139 S. Davies, Y. Hu, J. Blyth, N. Jiang and A. K. Yetisen, *Adv. Funct. Mater.*, 2023, **33**, 2214197.
140 J. Park, J. Kim, S.-Y. Kim, W. H. Cheong, J. Jang, Y.-G. Park, K. Na, Y.-T. Kim, J. H. Heo and C. Y. Lee, *Sci. Adv.*, 2018, **4**, eaap9841.
141 T. Arakawa, K. Tomoto, H. Nitta, K. Toma, S. Takeuchi, T. Sekita, S. Minakuchi and K. Mitsubayashi, *Anal. Chem.*, 2020, **92**, 12201–12207.
142 L. Garcia-Carmona, A. Martin, J. R. Sempionatto, J. R. Moreto, M. C. Gonzalez, J. Wang and A. Escarpa, *Anal. Chem.*, 2019, **91**, 13883–13891.